Ammonia/ionic liquid based double-effect vapor absorption refrigeration cycles driven by waste heat for cooling in fishing vessels

Wang, Meng; Becker, Tim; Schouten, Bob; Vlugt, Thijs; Infante Ferreira, Carlos

DOI
10.1016/j.enconman.2018.08.060

Publication date
2018

Document Version
Final published version

Published in
Energy Conversion and Management

Energy Conversion and Management 174 (2018) 824–843

Contents lists available at ScienceDirect

Energy Conversion and Management

journal homepage: www.elsevier.com/locate/enconman

Ammonia/ionic liquid based double-effect vapor absorption refrigeration cycles driven by waste heat for cooling in fishing vessels

Meng Wang*, Tim M. Becker, Bob A. Schouten, Thijs J.H. Vlugt, Carlos A. Infante Ferreira

Process and Energy Department, Delft University of Technology, Leeghwaterstraat 39 2628 CB Delft, The Netherlands

ARTICLE INFO

Keywords:
Double-effect absorption refrigeration cycle
Ionic liquid
Ammonia
Monte Carlo simulation
Fishing vessel
Waste heat recovery

ABSTRACT

To use high-temperature waste heat generated by diesel engines for onboard refrigeration of fishing vessels, an ammonia-based double-effect vapor absorption refrigeration cycle is proposed. Non-volatile ionic liquids are applied as absorbents in the double-effect absorption system. In comparison to systems using ammonia/water fluid, the complexity of the system can be reduced by preventing the use of rectification sections. In this study, a multi-scale method is implemented to study the proposed system, including molecular simulations (the Monte Carlo method) for computing vapor-liquid equilibrium properties at high temperatures and pressures, thermodynamic modeling of the double-effect absorption cycles, and system evaluations by considering practical integration. The Monte Carlo simulations provide reasonable vapor-liquid equilibrium predictions. 1-butyl-3-methylimidazolium tetrafluoroborate is found to be the best performing candidate among the investigated commercialized ionic liquids. In the proposed cycle, the best working fluid achieves a coefficient of performance of 1.1 at a cooling temperature of −5 °C, which is slightly higher than that obtained with generator-absorber cycles. Integrated with the exhaust gas from diesel engines, the cooling capacity of the system is sufficient to operate two refrigeration seawater plants for most of the engine operating modes in high-latitude areas. Thereby, the carbon emission of onboard refrigeration of the considered fishing vessel could be reduced by 1633.5 tons per year compared to the current practice. Diagrams of vapor pressures and enthalpies of the studied working fluids are provided as appendices.

1. Introduction

Global warming is one of the critical issues of the society in this age. According to the International Maritime Organization [1], maritime transport emits around 1000 million tons of carbon dioxide (CO_2) annually and is responsible for about 2.5% of global greenhouse gas emissions along with 15% and 13% of global NO_x and SO_x emissions. Fishery is one of the major parts of the maritime transport sector. Vessels for pelagic seas usually demand refrigeration plants, which consume fuel or electricity onboard [2]. The refrigeration plant is one of the largest electricity consumers onboard of fishing vessels, typically using 50% of the total power [3]. Diesel engines are normally used for propulsion and on-board electricity generation in trawlers. The engines also produce a significant amount of waste heat [4]. A study [5] shows that a large 2-stroke marine diesel engine may waste 50% of total fuel energy and 25.5% of the total energy is wasted through the exhaust gas (250–500 °C) [2].

Heat activated vapor absorption refrigeration (VAR) systems provide opportunities to recover waste heat and to use it to cool down fish and onboard space. Fernández-Seara et al. [6] designed, modeled, and analysed a gas-to-thermal fluid waste heat recovery system based on an ammonia/water (NH_3/H_2O) cycle for onboard cooling applications. Cao et al. [7] carried out a study on a water/lithium bromide (H_2O/LiBr) VAR system powered by waste heat for space cooling in a cargo ship. In their study, the cooling *COP* is 0.6 and an electricity-based coefficient of performance (*COP*) could be up to 9.4. Thereby, fuel consumption and CO_2 emission for the cooling system are reduced by 62%. Recently, Salmi et al. [4] modeled both an H_2O/LiBr single-effect (SE) VAR cycle and an NH_3/H_2O refined cycle for cooling on a bulk carrier ship with waste heat recovered from exhaust gases, jacket water and scavenge air cooler. The VAR system has a theoretical potential to save 70% of electricity in comparison to a compression air-conditioning system. They also pointed out that the H_2O/LiBr cycle is more efficient (*COP* of 0.75–0.85) and NH_3/H_2O is more suitable for below-freezing-point cooling (*COP* of 0.5).

Exhaust gases seem to be the best source of waste heat onboard to drive absorption chillers, even though they cannot be cooled down below 167 °C because of a risk of sulfur corrosion [4]. At temperatures above

* Corresponding author.
E-mail address: M.Wang-2020@outlook.com (M. Wang).

https://doi.org/10.1016/j.enconman.2018.08.060
Received 6 December 2017; Received in revised form 13 August 2018; Accepted 16 August 2018
Available online 30 August 2018

Nomenclature

COP	coefficient of performance [–]
c_p	specific heat capacity [kJ/(kg K)]
DR	distribution ratio [–]
f	circulation ratio [–]
h/Δ*h*	specific enthalpy (difference) [kJ/kg]
k	scaling parameter [–]
M	a notation of densities or heat capacities in Eq. (2) [–]
Mw	molecular weight [kg/kmol]
$\dot{m}$	mass flow rate [kg/s]
P	pressure [bar]
$\dot{Q}$	heat load [kW]
q	quality [–]
R	ideal gas constant [8.314472 J/(mol K)]
T	temperature [°C or K]
$\dot{W}$	power [kW]
w	mass fraction [–]
x	mole fraction [–]
Z	compressibility [–]

Greek symbols

α	parameter in the NRTL model [–]
ϵ	Lennard-Jones energy parameter [–]
η	efficiency [–]
ρ	density [kg/m^3]
τ	parameter in NRTL model [–]

Subscript and superscript

1, 2…	state point
abs	absorption
c	critical point
con	condensation/low pressure condensation
eva	evaporation
ex	exhaust gas
gen	generation
hpg	high pressure generation
i	inlet
ig	ideal gas properties
IL	ionic liquid component
lc	low pressure condenser
lg	low pressure generator
mix	mixing properties
NH_3	NH_3 component
o	outlet
onset	onset
p	pump
sat	properties of a saturated system
sol	solution
sub	properties of a supercooled system
whr	recovered waste heat
V	vapor

Abbreviation

ABS	absorber
CON	condenser
CWP	chilled water plant
DE	double-effect
EVA	evaporator
EXP	experimental (data)
FP	freezing plant
GAX	generator-absorber heat exchange
GEN	generator
HC	high pressure condenser
HG	high pressure generator
HX	heat exchanger
iHX	intermediate heat exchanger
IL	ionic liquid
LG	low pressure generator
MC	Monte Carlo
NRTL	non-random two-liquid activity coefficient model
REC	rectifier
RSW	refrigeration seawater (plant)
SE	single-effect
SHX	solution heat exchanger
SIM	simulated (data)
VAR	vapor absorption refrigeration
VLE	vapor-liquid equilibrium/vapor-liquid equilibria
WHR	waste heat recovery
[bmim][BF_4]	1-butyl-3-methylimidazolium tetrafluoroborate
[emim][Tf_2N]	1-ethyl-3-methylimidazolium bis(trifluoromethylsulfonyl) imide
[emim][SCN]	1-ethyl-3-methylimidazolium thiocyanate

150 °C, double-effect vapor absorption refrigeration (DE-VAR) cycles, in which the refrigerant is generated twice, are able to achieve higher thermal efficiencies by taking advantage of the higher temperature of the heat sources [8]. However, these cycles usually utilize the working fluid H_2O/LiBr, which cannot meet the demand of below-freezing-point cooling. With NH_3/H_2O, the DE-VAR is not feasible because of the need of rectifiers which introduce a higher complexity.

To use higher temperature exhaust gases for below-freezing-point cooling onboard, NH_3 with ionic liquids (ILs) working fluids is proposed to be used in DE-VAR systems. ILs, a family of room-temperature molten salts, have been intensively studied due to their potential in replacing the absorbents in conventional absorption refrigeration and heat pump technology [9]. ILs show strengths such as high boiling points, strong affinities with refrigerants and high chemical and thermal stabilities [9]. Moreover, NH_3 based absorption systems have strengths such as below-freezing-point cooling, free of air infiltration and low impact on the environment (zero for both ozone depletion and global warming potentials).

NH_3/ILs working fluids in absorption cycles have received significant attentions in the past decade. Yokozeki and Shiflett [10] reported the first vapor-liquid equilibrium (VLE) data of four NH_3/ILs working pairs. By including measurements and correlations of the other four NH_3/ILs pairs, the performance of the eight NH_3/ILs fluids in an SE absorption cycle was compared in Ref. [11]. Most of their studied imidazolium ILs are currently well commercialized. Functional ILs with NH_3 in SE absorption cycles were also investigated. For instance, Chen et al. [12] investigated the VLE property of NH_3 with a metal ion-containing imidazolium IL. A thermodynamic performance of a VAR cycle using the studied fluids was conducted in a sequential work by the same authors [13]. Ruiz et al. [14] studied some ammonium ILs. Cera-Manjarres [15] explored six other ILs including imidazolium and ammonium ILs with a hydroxyl group (-OH). By applying more reliable mixing enthalpies and experimental heat capacities, Wang and Infante Ferreira [16] explored the performance of nine NH_3/ILs fluids in SE absorption cycles for heat pump systems. The authors identified promising absorbents which work with NH_3 in absorption cycles under 130 °C heating.

Nevertheless, the above studies were all applied at temperature and pressure ranges available for SE-VAR cycles. The DE-VAR cycle requires

VLE data at higher temperatures and higher pressures, which have not been measured experimentally. Previously, Wang and Infante Ferreira [17] investigated nine NH_3/ILs working fluids in DE absorption cycles for application in refrigeration and heat pump systems. The used VLE properties were obtained by simply extrapolating the ones at temperatures and pressures available for SE-VAR cycles. Schouten [18] used the same extrapolated properties for a DE-VAR in a series design. In this context, Becker et al. [19] showed that molecular simulation is able to predict relevant thermophysical properties for temperatures and pressures applied in SE-VAR cycles. These authors also pointed out that improved force fields are needed for an accurate prediction of the cycle performance.

In this work, a DE-VAR in parallel configuration using NH_3/ILs fluids is proposed for refrigeration applications in fishing vessels, driven by heat recovered from diesel engines. A multi-scale method is applied to study its performance, from a molecular level to a system integration level, as shown in Fig. 1. First, an adjusted force field is used in Monte Carlo (MC) simulations to predict VLE properties in high temperature and high pressure conditions of the three selected NH_3/IL pairs. Together with the experimental VLE and heat capacities, the VLE data are correlated and mixture enthalpies are predicted. These thermophysical properties are then used for the evaluation of the DE-VAR cycles. After considering practical concerns, a case study based on a real vessel operating in high-latitude conditions is carried out to check the techno-economic feasibility of the integrated system in practice.

2. Properties of working fluids

In this study, the ILs under consideration are 1-ethyl-3-methylimidazolium thiocyanate ([emim][SCN], CAS registry No. 331717-63-6), 1-butyl-3-methylimidazolium tetrafluoroborate ([bmim][BF4], CAS registry No.174501-65-6) and 1-ethyl-3-methylimidazolium bis(trifluoromethylsulfonyl) imide ([emim][Tf_2N], CAS registry No.174899-82-2). The corresponding NH_3/IL working fluids were identified showing higher *COP*s than NH_3/H_2O in SE absorption cycles [16]. Additionally, as commercialized ILs, their thermophysical properties and force fields required in this study are accessible. Hence, they are selected as the investigated ILs.

2.1. Vapor-liquid equilibrium properties for the binary solutions

For three studied NH_3/IL working fluids, experimental VLE data measured by Yokozeki and Shiflett [10,11] only cover the conditions suitable for SE-VAR cycles. To extend the VLE data of these fluids for DE-VAR cycle at higher temperature and pressure conditions, Monte Carlo simulations are conducted. The data from experimental sources together with the simulated ones are correlated with the NRTL model for usage in the studied cycle.

2.1.1. Monte Carlo method

Molecular simulation is a powerful tool to predict the behavior of materials [20]. In this type of simulation, thermodynamic properties are computed based on force fields which describe interactions between molecules [21]. Comparable to the previously discussed models, these force fields are often developed by correlating experimental data. However, the potential to predict properties outside the correlated data is often better than with traditional models and hence molecular simulations can be used to extend existing experimental data [22]. Here, MC simulations were performed to obtain solubility data of NH_3 in 3 different ILs at higher temperatures than measured experimentally.

As shown in a previous publication by the authors [19], the osmotic ensemble [23] can be applied to compute the uptake of gases in ILs. Thereby, the temperature, the pressure, the number of solvent molecules, and the fugacity of the solute are fixed, while the volume of the system, and the number of solute molecules can fluctuate. Here, the Continuous Fractional Component Monte Carlo method is applied to insert and delete solute molecules [24]. After the equilibration phase, the total amount of solute molecules in the system determines the gas uptake at the chosen conditions. The details of the conducted simulations can be found in the previous work by the authors [19].

All force fields considered in this work were taken from literature. The force fields for the ILs were taken from the work of Tenney et al. [25] (for cation [$emim^+$] and anion [SCN^-]), Liu et al. [26] (for cation [$bmim^+$] and anion [Tf_2N^-]), and Canongia Lopes and Pádua [27] (for anion [BF_4^-]). For NH_3, the TraPPE force field was used [28]. In the simulations, parts of the cations and NH_3 molecules are considered to be rigid while the alkyl part and the anions are flexible. A summary of the force field parameters is provided in the Supplementary Information. The Ewald summation technique with a relative precision of 10^{-5} [20] is used to calculate electrostatic interactions. Lennard-Jones interactions are truncated and shifted at 12 Å without applying tail corrections. Polarization is not explicitly considered in the simulations. The simulations are conducted with the RASPA software package [29].

Unfortunately, commonly used force fields do not predict the solubility of NH_3 in ILs accurately [19]. To overcome this limitation, the binary mixing rule of the Lennard-Jones energy parameters, ϵ, between

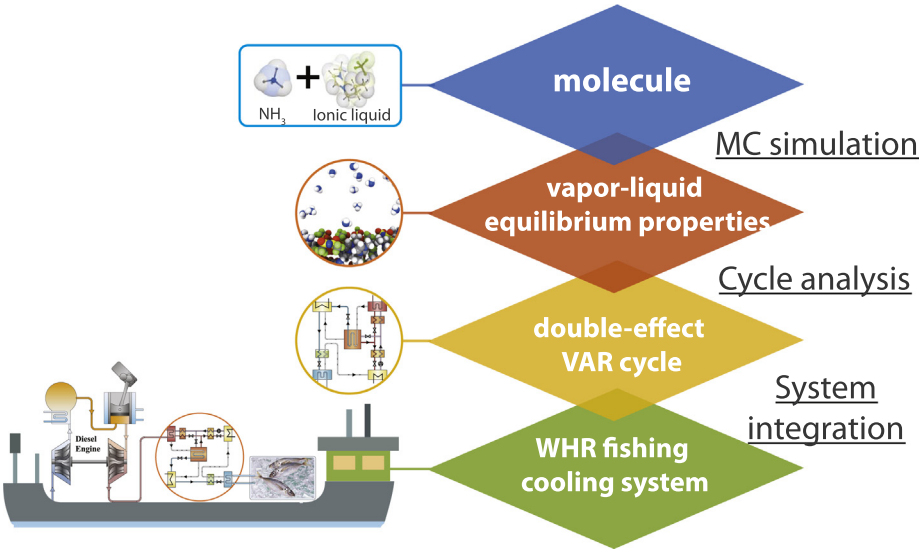

Fig. 1. Outline of this study showing different levels of details considered.

NH_3 and ILs in MC simulations, has been scaled to fit the experimental solubility for available conditions. The applied mixing rule is:

$$\epsilon = k \cdot \sqrt{\epsilon_{NH_3} \cdot \epsilon_{IL}} \quad (1)$$

By adjusting ϵ, the interaction strength between NH_3 and the ILs is changed. Different interaction strengths between the molecules were tested to find the one that predicts the best behavior in regard to the experimental data. The applied scaling parameter, k, is respectively 0.78, 0.15, and 0.78 for [emim][SCN], [bmim][BF_4] and [emim][Tf_2N]. To validate the quality of the adjusted force field, a comparison between the computed solubilities (dashed curves) with the adjusted force fields and the experimental data [10,11] (solid curves) is provided in Fig. 2.

In the case of [bmim][BF_4] (Fig. 2(b)), the computed solubility without adjusting force field is also shown (dotted curves). It can be observed that the qualitative trend of the gas uptake of these simulations is similar, while the absolute values are significantly overestimated. After the scaling of the mixing rule, the simulation results agree well with the experimental data for all investigated ILs and for varying temperatures. The average 95% confidence interval for the computed solubilities for [emim][SCN], [bmim][BF_4], and [emim][Tf_2N] used in the cycle calculations is 2.8%, 1.7%, and 2.9%, respectively.

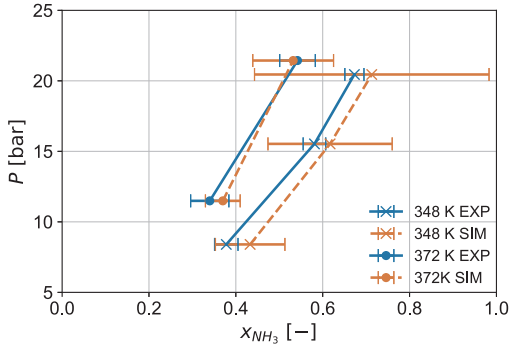

(a)

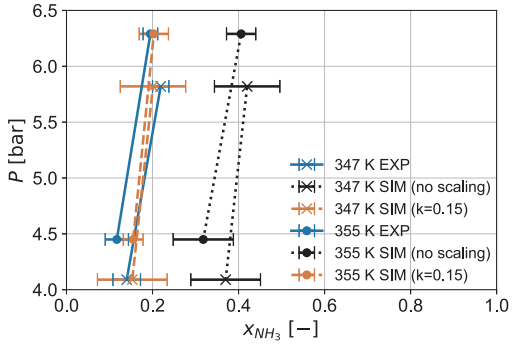

(b)

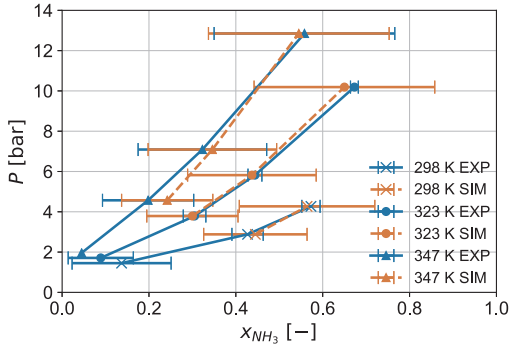

(c)

Fig. 2. Comparison between the simulated (SIM) and experimental (EXP) VLE data [10,11] with error bars for the working pairs: (a) NH_3/[emim][SCN], (b) NH_3/[bmim][BF_4] and (c) NH_3/[emim][Tf_2N]. The shown error bars of the simulated data represent the 95% confidence interval.

2.1.2. Correlations of vapor-liquid equilibrium properties

The non-random two-liquid (NRTL) model has been shown as a suitable model to correlate and predict VLE of ILs-based working fluids [30]. The experimental vapor pressures of NH_3/IL binary systems have been regressed to the NRTL model as explained by Wang and Infante Ferreira [16]. Subsequently, the operating concentrations of solutions can be determined. The form of the NRTL model can be found in Ref. [16]. Note that for the data points at temperatures above the critical point of NH_3, an extrapolation of the vapor pressure equation is used for an easy processing of the data [13]. In particular, an extrapolation of the Antoine equation is applied. This processing will somehow influence the solid physical basis of the NRTL model.

2.2. Densities and heat capacities

Densities of pure [emim][SCN], [bmim][BF_4] and [emim][Tf_2N] have been reported by Matkowska and Hofman [31]; Ficke et al. [32], Tariq et al. [33] respectively. Specific heat capacities of [emim][SCN] are from the work of Navarro et al. [34]. The data reported by Paulechka et al. [35] and Nieto de Castro et al. [36] are used together for the specific heat capacities of [bmim][BF_4]. For [emim][Tf_2N], the data of specific heat capacities were reported by Paulechka et al. [37] and Ferreira et al. [38] for different temperature ranges. These data are plotted in Fig. 3, as functions of temperature. Correlations of the data are listed in Table 1.

Currently, densities and heat capacities of the studied NH_3/IL mixtures have not been reported. Eq. (2) provides a general form of ideal solution properties, which is based on a weighted average of properties from both components. This form is used to estimate the densities and heat capacities for the investigated mixtures:

$$M_{sol} = w_{NH_3} M_{NH_3} + w_{IL} M_{IL} \quad (2)$$

This simplification is verified with the density data of six NH_3/IL mixtures reported by Cera-Manjarres [15]. The maximum relative deviation is 6.5%. Moreover, the simplification for the heat capacities has been verified with data of H_2O/[mmim][DMP] from Dong et al. [39]. The relative deviation is smaller than 4% [16]. This treatment has also been checked by the authors for the H_2O/[emim][DMP] solution, for predicting the solution enthalpy and cycle performance. No obvious difference has been observed in comparison to using the heat capacity of the real solutions [30].

2.3. Enthalpies

The enthalpy of pure NH_3 is directly obtained from NIST's Refprop [40].

For a saturated solution at T, P and with an NH_3 mass fraction of w_{NH_3}, the total enthalpy of the solution, h_{sat}^{sol}, is provided by,

$$h_{sat}^{sol}(T, P, w_{NH_3}) = w_{NH_3} h_{NH_3}(T) + w_{IL} h_{IL}(T) + \Delta h_{mix}(T, P, w_{NH_3}) \quad (3)$$

where the enthalpies of NH_3 are chosen at their saturated liquid states for the cases below the critical temperature. For the cases at temperature above the critical point of NH_3, an additional effect of ideal gas enthalpy is added to the enthalpy at the critical point, following the work of Chen et al. [13]:

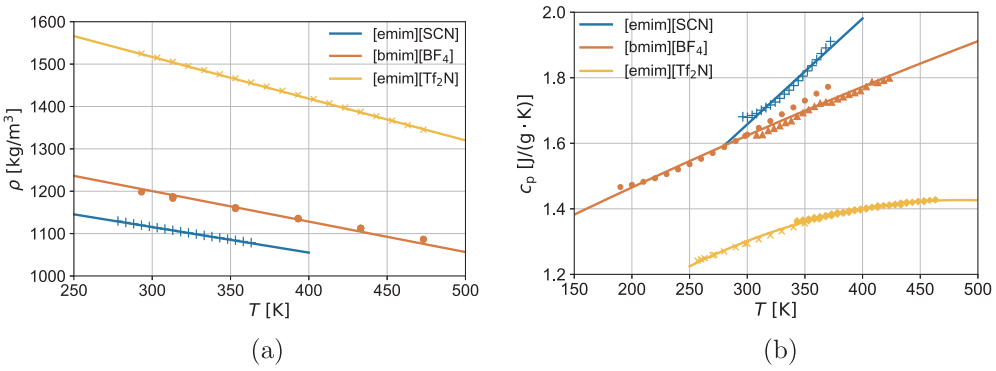

Fig. 3. Experimental data and the correlations of (a) densities [31–33], and (b) heat capacities [34–38] of the three studied ILs.

Table 1
Molecular weights (*Mw*) and correlations of relevant thermophysical properties for the 3 investigated ILs at 1 bar *.

IL	*Mw* [kg/kmol]	ρ [kg/m^3]	c_p [kJ/(kg K)]
[emim][SCN]	169.25	$\rho = 1296 - 0.602 \times T$	$c_p = 0.6882 + 0.0032 \times T$
[bmim][BF_4]	226.02	$\rho = 1416 - 0.719 \times T$	$c_p = 1.119 + 1.83 \times 10^{-3} \times T - 4.879 \times 10^{-7} \times T^2$
[emim][Tf_2N]	391.31	$\rho = 1812 - 0.9837 \times T$	$c_p = 0.5644 + 3.56 \times 10^{-3} \times T - 3.674 \times 10^{-6} \times T^2$

* T in K.

$$h_{NH_3}(T)|_{T>T_c} = h_{NH_3}(T_c) + \int_{T_c}^{T} c_{p,ig}^{NH_3} dT \quad (4)$$

For the ILs, enthalpies are calculated based on their pure heat capacities c_p^{IL},

$$h_{IL}(T) = h_0(T_0) + \int_{T_0}^{T} c_p^{IL} dT \quad (5)$$

The experimental mixing enthalpy Δh_{mix} used in Eq. (3) has not been reported for the studied NH_3/IL working fluids. For an alternative NH_3/IL working fluid, the authors have quantified this term using various thermodynamic models [30]. The calculation has shown that the exothermic effect of mixing NH_3/IL is less than that of mixing H_2O/IL. Furthermore, it has been shown that neglecting Δh_{mix} does not significantly change the total enthalpy and the *COP* in an SE-VAR cycle with NH_3/IL pairs [30]. Therefore, in the following calculations, the effect of the mixing enthalpy is neglected.

For solutions at a subcooled condition T, P and w_{NH_3}, enthalpies can be obtained by subtracting the subcooled part from corresponding saturated solution,

$$h_{sub}^{sol}(T, P, w_{NH_3}) = h(T_{sat}, P, w_{NH_3}) - \int_{T}^{T_{sat}} c_p^{sol} dT \quad (6)$$

3. Configurations of cycles and modeling methods

The configuration and modeling method of the studied DE-VAR cycle are presented. Besides, an alternative choice, the generator-absorber heat exchange (GAX) cycle with NH_3/H_2O, is introduced for a sake of comparison, since it is promising with high temperature heat sources [8].

3.1. Double-effect absorption refrigeration cycle

Fig. 4 depicts a schematic representation of a double-effect absorption system in parallel configuration. The main feature of the parallel DE-VAR cycle is that the strong solution (strong in refrigerant NH_3), pumped from the absorber (ABS), is divided into two parallel streams after being heated in the solution heat exchanger (SHX1).

Two sub-streams are heated in two generators (GENs) to generate refrigerant vapor: One of the sub-streams is heated in the high pressure generator (HG) by the external heat source at a high temperature. Superheated refrigerant vapor is generated there and then continues to the high pressure condenser (HC). The other sub-stream is heated in the low pressure generator (LG) to generate the other refrigerant vapor. The heat is from the condensation of the superheated refrigerant vapor in the HC. The HC and LG are coupled in an intermediate heat exchanger (iHX).

Key state points of the solutions are illustrated qualitatively in both ln *P*-(-1/*T*) and *h*-*w* diagrams in Fig. 5. The cycle 5-8-9-11a-11-13-5 shows the sub-stream passing the HG and cycle 5-7c-11b-11-13-5 represents the other sub-stream passing the LG.

The mass flows of the two sub-streams of the solution can be quantified with the distribution ratio (*DR*), which is defined as the mass flow ratio between the sub-stream of the solution passing the HG and the total mass flow:

$$DR = \frac{\dot{m}_8}{\dot{m}_5} \quad (7)$$

3.2. Modeling method of the cycle

To create an integrated model for the thermodynamic analysis of the DE-VAR system, several assumptions are made to simplify the calculations:

- The system operates in a steady state.
- The operating pressures of the absorber and the evaporator are identical, and similarly, the pressure of each generator is equal to its directly linked condenser.
- In the outlets of the two condensers and evaporator, the refrigerant stream is in a saturated liquid or saturated vapor state, respectively. The solution is in equilibrium state while leaving two generators and the ABS.
- The pinch temperature of the SHXs is assumed as 10 K. The pinch temperature of the iHX is set to 5 K. The effectiveness of the HX1 is assumed to be 75%.
- Heat losses and pressure losses are neglected.
- Throttling is an isenthalpic process.

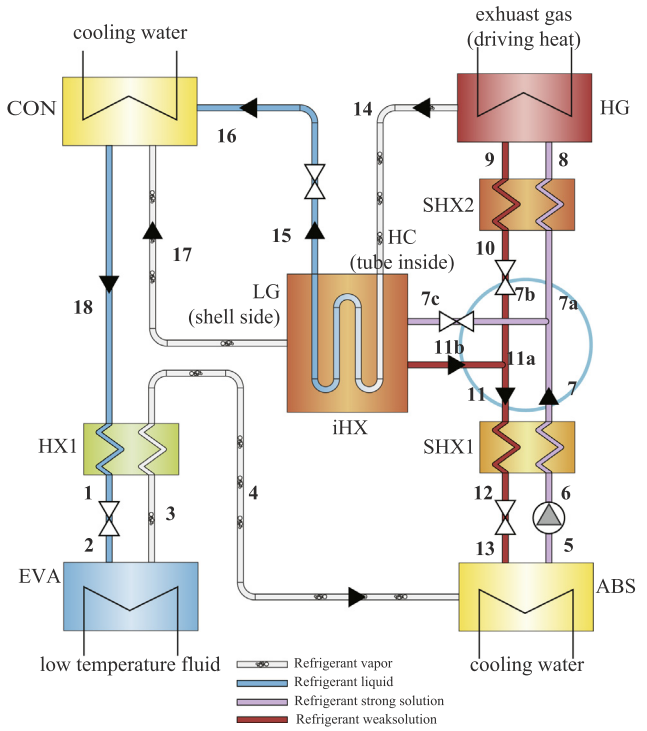

Fig. 4. Schematic diagram of the studied DE-VAR system in parallel configuration. Non-volatile absorbents absorb refrigerant in the absorber (ABS). The solutions are then pumped parallelly to the high and low pressure generators (HG and LG) for refrigerants generation. A blue circle identifies the parallel substreams leaving and returning the ABS. The refrigerant vapors generated in the HG are used for heating the LG. The two refrigerant streams are mixed in the condenser (CON) and then go through the valve and the evaporator (EVA) to generate cooling effects.

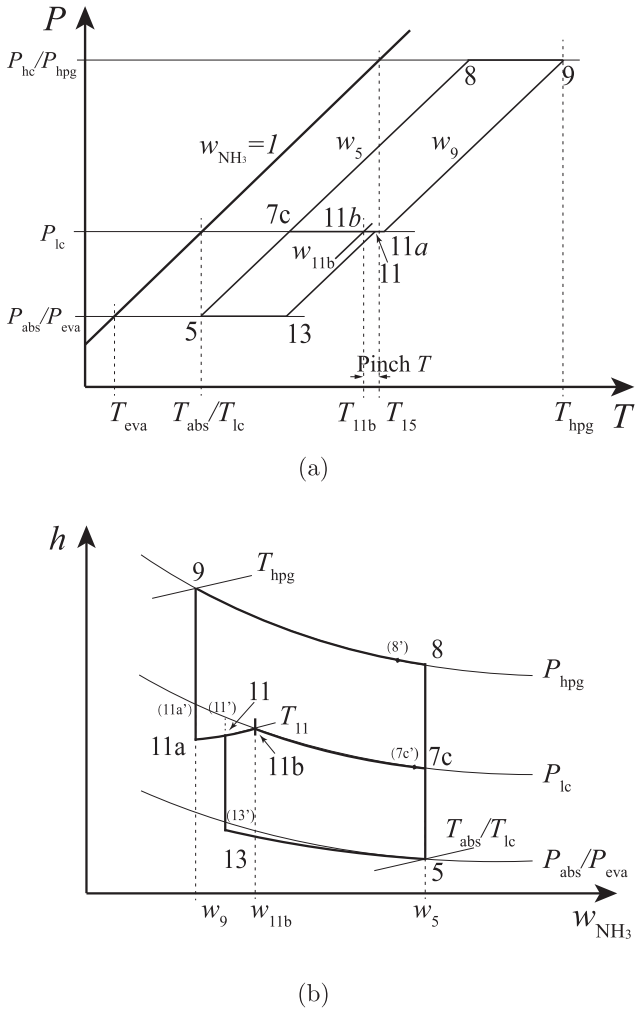

Fig. 5. The state points (referring to the points shown in Fig. 4) of the solution stream plotted in a $\ln P-(-1/T)$ diagram (a) and an $h-w$ diagram (b). Points 11, 11a and 13 sharing the same pressure and fraction with points 11', 11a', and 13', respectively, are at subcooled conditions. Points 7c and 8 have a possibility of refrigerant boil off, the portions of saturated solutions are denoted as 7c' and 8.', respectively.

For each component shown in Fig. 4, the mass, species and energy balances are implemented. For instance, for the ABS shown in Fig. 4, the balances are:

$$\begin{cases} \dot{m}_4 + \dot{m}_{13} = \dot{m}_5 \\ \dot{m}_4 + w_{13}\dot{m}_{13} = w_5\dot{m}_5 \\ \dot{m}_4 h_4 + \dot{m}_{13}h_{13} = \dot{m}_5 h_5 + \dot{Q}_{abs} \end{cases} \tag{8}$$

The power consumption of the solution pump, $\dot{W}_p$, can be calculated by,

$$\dot{W}_p = \frac{\dot{m}_5}{\rho_{sol}} \frac{P_{hpg} - P_{eva}}{\eta_p} \tag{9}$$

The calculation procedure for the cycle is illustrated in Fig. 6. The temperature of state point 7, which is between two SHXs, is obtained iteratively to reach the energy balances of both the SHXs. The other iteration is required to determine the temperature of state point 15, which is based on the energy balance of the iHX.

With the heat duties and the pump power consumption, the coefficient of performance, *COP*, of a cycle for cooling is defined as,

$$COP = \frac{\dot{Q}_{eva}}{\dot{Q}_{hpg} + \dot{W}_p} \tag{10}$$

The circulation ratio, f, defined as the required mass flow of pump stream for generating a unit mass flow of refrigerant, is also taken into account in this study. f can be obtained via mass and species balances around the ABS as,

$$f = \frac{\dot{m}_5}{\dot{m}_4} = \frac{1 - w_{13}}{w_5 - w_{13}} \tag{11}$$

This model was previously validated by Vasilescu and Infante Ferreira [41] for an air-conditioning application with an LiBr/H_2O working pair.

3.3. Generator-absorber heat exchange cycle

NH_3/H_2O GAX cycles have been claimed to be suitable for applications with higher temperature driving heat [8]. As shown in Fig. 7, the promising thermal performance of this cycle is achieved by coupling the heat between partial sections of the GEN and the ABS.

A perfect operation of the GAX cycle relies on the accurate identifying of temperature profiles of sections in ABS and GEN where the heat can be coupled. This kind of heat coupling is difficult to achieve in practice. However, the GAX cycle represents "a compelling theoretical possibility" [8]. Therefore it is used as a benchmark to compare the DE-VAR cycle with.

The modeling of the GAX cycle is based on the method introduced by Herold et al. [8]. During the heat coupling, both the available heat in the ABS and the required heat in the GEN can be obtained through mass and energy balances, by assuming that solution and vapor streams in the ABS or GEN are in counter-current flow, and the solutions streams of the ABS and GEN are also in counter-current flow. The GAX heat really transferred is the minimum between the available and required heat of vapor generation. The rectifier is analyzed as an ideal device

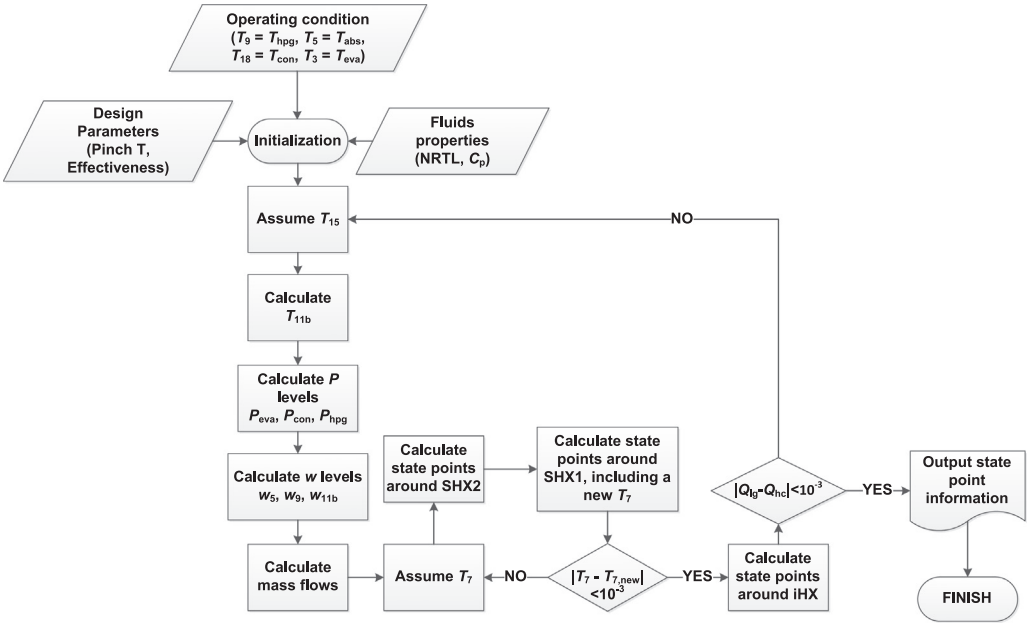

Fig. 6. Flow-chart for the thermodynamic modeling of the DE-VAR in parallel configuration. Mass, species and energy balances are applied in each component. Iterations of T_{15} and T_7 are implemented to reach the balances of the iHX and two SHXs.

that produces vapor with 99.5% NH_3.

4. The integrated fishing vessel

A trawler vessel is taken into consideration for the following case studies.

The required cooling capacity in this vessel is provided by the refrigeration seawater (RSW) plant, chilled water plant (CWP), and freezing plant (FP). Currently, the plants are all configured with vapor compression refrigeration systems. The RSW and CWP apply NH_3 as a refrigerant, while FP is an NH_3/CO_2 cascade system (NH_3 is used in the high temperature circuits). The technical characteristics are listed in Table 2. It is investigated if the proposed IL-based DE-VAR system has the potential to replace the current plants entirely or partially.

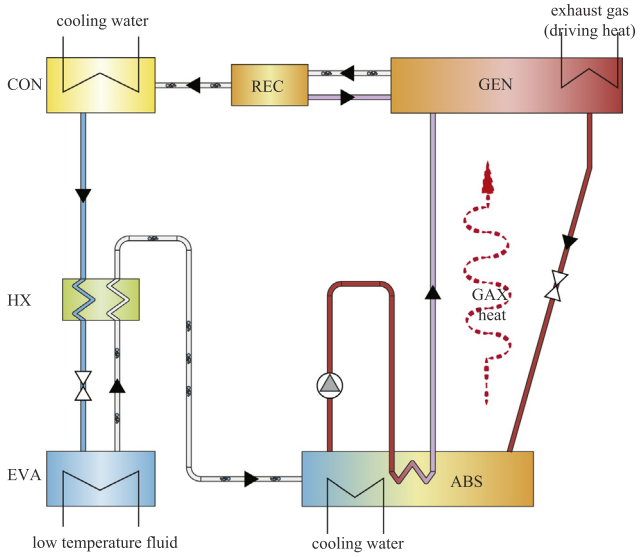

Fig. 7. Schematic diagram of a standard NH_3/H_2O GAX system [8]. The main feature of the GAX cycle is that the final stages of its ABS have higher temperatures than the flow in the first stages of the GEN. The heat from the ABS can be recycled to heat up those stages in the GEN. The weak NH_3/H_2O solutions absorb NH_3 vapors from the EVA and experience an internal heat recycling in the ABS before they are pumped into the GEN. Vapors leaving the GEN are mixtures of NH_3/H_2O, which are purified in the rectifier (REC). The NH_3 vapors then experience the similar process as the DE-VAR cycle for generating cooling effects.

Scavenge air, jacket water, and exhaust gas are among the main waste heat sources from the diesel engines as illustrated in Fig. 8. The heat released via the exhaust gas takes up approximately 50% of total wasted heat [5]. In this study, the exhaust gas after the turbine is used.

The studied ship is equipped with a Wärtsilä diesel engine of type 12V38 for propulsion [42]. The properties of the exhaust gas after the turbine from this engine are shown in Fig. 9, which are taken from the official project guide [42]. Note that the data for 40% load are based on extrapolations.

Operations of the engine can be classified into the five typical modes, which are listed in Table 3. Corresponding exhaust gas properties are identified from Fig. 9.

5. Results and discussion

Following the proposed multi-scale method, the result of the property level, cycle level, and integrated system level are discussed in this section.

5.1. Simulation of vapor-liquid equilibrium properties and their correlations

The experimental VLE data and the ones from Monte Carlo

Table 2
Cooling capacities, temperatures and power consumptions of the refrigeration plants (RSW, CWP and the NH_3 circuits of FP) used in the studied trawler vessel, in two typical climate cases.

	$\dot{Q}_{eva}$ [kW]	T_{eva} [°C]	$\dot{W}$ [kW]	
RSW plant	2×1416	−5	2×414	32 °C heat sink
CWP	2×880	−5	2×222	
FP (NH_3 circuits)	2×900	−5	2×253	
RSW plant	2×1556	−5	2×271	16 °C heat sink
CWP	2×954	−5	2×152	
FP (NH_3 circuits)	–	–	–	

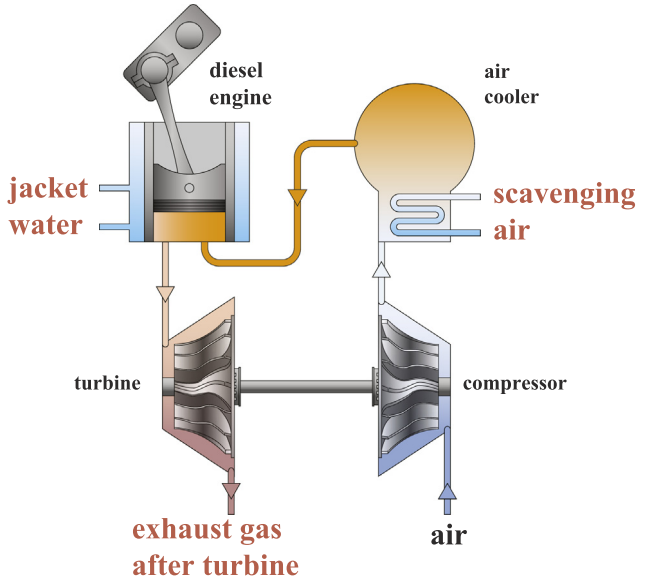

Fig. 8. Main waste heat sources of a two-stroke diesel engine: Scavenge air is used to cool down the compressed air before going to the engine. Jacket water is applied to maintain the temperature of the engine where the combustion of fuels takes place. Exhaust gas, a mix of air and fuel at high temperature, is released with 50% of the total waste heat.

simulations are plotted together in Fig. 10 for the three studied NH_3/IL working fluids.

The fitted parameters of the NRTL model based on the shown data are listed in Table 4. These parameters follow the same notations introduced in Ref. [16].

Based on the NRTL model, predicted vapor pressures of the three studied fluids are shown in Fig. 11. To show the influence of the additional data provided by the Monte Carlo simulations, the results are compared with and without the inclusion of the computed data. Vapor pressures shown in Fig. 11(a), (c) and (e) are obtained by only fitting experimental VLE data at low temperatures and low pressures (interaction parameters can be found in Ref. [16]). The vertical and horizontal dashed lines represent temperature and pressure boundaries, respectively, of EXP data. The other three diagrams are based on both the experimental VLE data and the computed ones. In each diagram of Fig. 11, NH_3 fractions represented by the various curves cover the conditions applied in the DE-VAR cycle.

Vapor pressures fitted only with the VLE data at low temperatures and low pressures (Fig. 11(a), (c) and (e)) show linear behavior inside the experimental temperature and pressure ranges. However, out of the

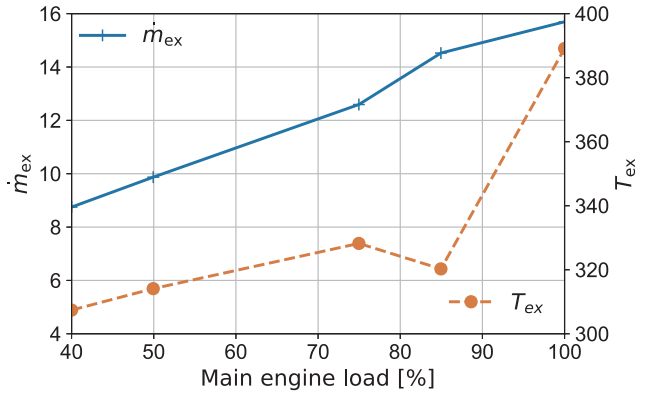

Fig. 9. Exhaust gas flow and temperature (after the turbine) of the studied diesel engine 12V38 for different engine loads [42]. The solid curve denotes the flow rate of the exhaust gas and the dashed curve denotes its temperature after the turbine.

range of the experimental data, the vapor pressures increase rapidly with an increase of temperature. This behavior fails to follow the physical basis indicated by the Clausius-Clapeyron equation (Eq. (12)): for which the vapor pressures are approximately linear, because the term $-\Delta h/(R\Delta Z)$ depends only slightly on temperature [43].

$$\frac{d\ln P}{d(1/T)} = -\frac{\Delta h}{R\Delta Z} \tag{12}$$

The nonlinear shape of vapor pressures curves is pronounced at relatively low NH_3 mass fractions, which are crucial for the studied cycle. The influence of using exclusively the experimental based VLE properties on estimating the cycle performance will be discussed in detail in Section 5.3.2.

By including the computed data (right-hand side), the trends of vapor pressures, especially for the cases with low NH_3 fractions at high temperatures, become more reasonable. This indicates that the simulation helps to improve the description of the behavior. The reasonable extension of the VLE data for NH_3/IL mixtures, confirms the added value and need for MC simulations to extend the range of VLE properties of NH_3/IL mixtures.

5.2. Diagrams of thermophysical properties

Based on the thermal property methods discussed in Section 2, the diagrams of the studied working fluids are generated for using them in thermal applications including VAR cycles. The corresponding diagrams are provided in the Appendix.

5.3. Cycle performance

With the thermo-physical properties, the performance of the DE-VAR cycle can be predicted. The influences of operation conditions and different sources of properties are investigated. The comparison of its performance with the GAX cycle is also presented.

5.3.1. The influence of varying operation conditions

Parametric studies are carried out to explore the performance of the DE-VAR for different operating conditions. The investigated parameters are the *DR*, the heat source temperature, the cooling temperature and the environmental temperature.

As shown in Fig. 12, optimum performances for different conditions (heat source temperature, T_{hpg}, of 160 and 220 °C, respectively) of the three working fluids are always obtained when the *DRs* are close to 0.5. This indicates that two sub-streams which are comparable in flow are preferable, which would allow for simplifications in constructing pipelines and controlling valves in a real system. In the following calculations, the value of *DR* will be kept constant at 0.5.

Fig. 12 also indicates that a higher temperature of the heat source, T_{hpg}, contributes to a better performance for the studied conditions. Similar trends can be observed for the other cases in Fig. 13(a) and (b) for which the cooling temperature, T_{eva}, is at a relatively low level or the heat sink temperature, T_{con} and T_{abs}, is at a relatively high level. However, when T_{eva} is higher and T_{con} or T_{abs} is lower, an increase of T_{hpg} can lead to constant trends of the *COP*. This is, for instance, the case in Fig. 13(a), when T_{eva} = 10 °C, for the working pair NH_3/[bmim][BF_4]. A decreasing trend can also be observed in Fig. 13(b), when T_{eva} = 0 °C, for the same working pair.

Fig. 13(a) and (b) indicate that a lower temperature of the cooling demand leads to an inferior performance for all working pairs. Moreover, for the same operating condition, the NH_3/[bmim][BF_4] pair performs better than the other two pairs.

The influence of the temperature of the seawater on the performance can be understood by comparing Fig. 13(a) and (b). Fig. 13(a) applies for cases in which the seawater temperature is 32 °C, corresponding to an application in tropical areas. The temperature of the working fluid side is 5 K higher than the cooling medium, the seawater

Table 3
Typical operating modes of the fishing vessel, main engine loads and the corresponding flow and temperature of the exhaust flue gas flow.

	Operation mode	Duration per year [hour]	Main engine load [–]	Exhaust gas flow [kg/s]	T of exhaust gas [°C]
Mode 1	Fishing with production	5400	90%	15	340
Mode 2	Fishing without production	400	90%	15	340
Mode 3	Sailing to fishing zone and pre-cooling	320	70%	12	326.5
Mode 4	Placing or retrieving nets, pumping fish on board	1200	40%	8.75	307.4
Mode 5	Unloading or out of service	1440	0%	–	–

(T_{abs} = T_{con} = 37 °C). Fig. 13(b) corresponds to an application in high-latitude areas, for instance, the North Sea adjoining the Netherlands, where the seawater temperature is on average 16 °C (T_{con} = T_{abs} = 21 °C).

The comparison of Fig. 13(a) and (b) shows that both working fluids have higher performances at lower T_{abs} and T_{con}. Unfortunately, for the application in tropical areas, the DE-VAR cycle with working pairs NH_3/[emim][SCN] and NH_3/[emim][Tf_2N] cannot operate at a cooling temperature of −5 °C. The NH_3/[bmim][BF_4] working fluid does not show very promising performance, either. Hence, the following analysis will only focus on high-latitude areas.

The DE-VAR cycle with NH_3/IL pairs shows similar performances, in respect to the operating conditions, as the cycle with the traditional H_2O/LiBr working pair [44] or other investigated working pairs, such as NH_3/$LiNO_3$ [45].

5.3.2. *The influence of different vapor-liquid equilibrium properties on the cycle performance*

To investigate the influence of excluding the simulated VLE data, the DE-VAR cycle with NH_3/[bmim][BF_4] in the condition of $T_{hpg}/T_{abs}/T_{con}/T_{eva}$ = 240/37/37/-5 °C is studied. Relevant parameters which can help to indicate the influences of different VLE sources on the cycle performance are listed in Table 5.

The NH_3 mass fractions of state point 5 (solution outlet of the ABS), 11b (solution outlet of the LG) and 9 (solution outlet of the HG) are determined by the temperatures and pressures at saturated conditions. The NH_3 fractions estimated based on solely extrapolating EXP VLE data are lower than those based on VLE data including SIM data (only for point 5, they are almost identical). From point 5 to 11b and to 9, temperatures and pressures increase. The deviation of saturated NH_3 fractions from the one obtained including SIM data also show an increasing trend.

Two streams with an NH_3 mass fractions of w_9 and w_{11b} are mixed before state point 13. Consequently, state point 13 also shows a lower value of NH_3 fraction when obtained without using the simulation VLE data. Due to the underestimation of the change in NH_3 fraction between points 5 and 13, the circulation ratio, f, which is based on w_{13} and w_5 (Eq. (11)), is lower than the one obtained using the SIM VLE. This indicates that the required pump flow is lower.

In terms of cycle performance, the specific heat duties and pump power are listed in Table 5, as well. They are the corresponding heat and power loads for 1 kg/s refrigerant flow. The estimated demands of heat and pump power by using exclusively EXP VLE data is underestimated compared with the ones using SIM VLE data. This is consistent with the underestimation of the circulation ratio. As a result, the COP is remarkably overestimated.

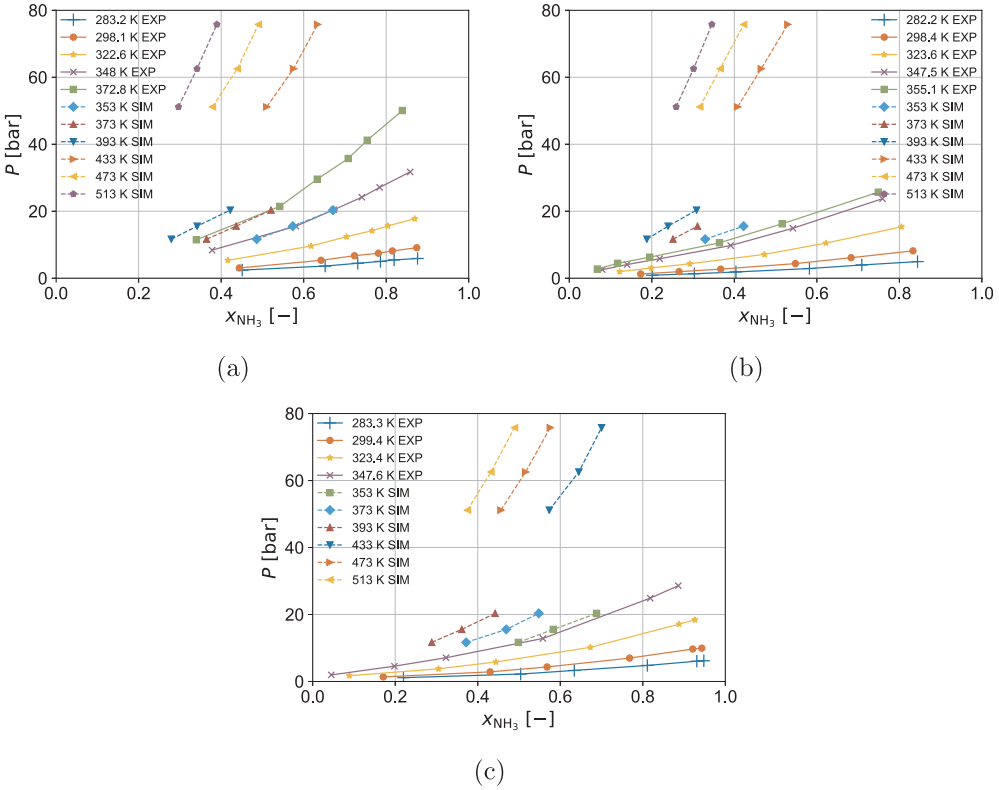

Fig. 10. VLE data of working pairs (a) NH_3/[emim][SCN], (b) NH_3/[bmim][BF_4] and (c) NH_3/[emim][Tf_2N]. Solid curves denote the experimental data from Yokozeki and Shiflett [10,11] (denoting as EXP), and dashed curves denote the simulated results by the authors (denoting as SIM).

Table 4
Fitted interaction parameters in the NRTL model (following the same notations in Ref. [16]) for the studied NH_3/IL working pairs.

IL	α [–]	$\tau_{12}^{(0)}$ [–]	$\tau_{12}^{(1)}$ [K]	$\tau_{21}^{(0)}$ [–]	$\tau_{21}^{(1)}$ [K]
[emim][SCN]	−0.0320	−20.18	4342.10	11.07	−2084.20
[bmim][BF_4]	−0.0001	−481.23	2740.10	456.75	−2297.27
[emim][Tf_2N]	−0.0024	−107.90	8969.70	82.95	−5276.93

5.3.3. Comparison with the generator-absorber heat exchange cycle

Fig. 14 shows how the *COP* of a GAX cycle changes with the temperature of the heat source, T_{gen}, at the condition of $T_{abs}/T_{con}/T_{eva}$ = 21/21/−5 °C. Due to the limitation of the thermophysical properties database [40] of the NH_3/H_2O mixture, the calculated performance of the GAX cycle can only be obtained for T_{gen} below 170 °C.

It can be seen in Fig. 14 that when T_{gen} is below 116 °C, there is no possibility for heat coupling. Thus, the GAX performs as a single-stage cycle, showing a decreasing trend with rising T_{gen}. Above 116 °C, the solid curve indicates the performance of the ideal GAX cycle, which is increasing as T_{gen} rises. The GAX cycle is entitled "ideal" because the calculation of it is based on the perfect heat coupling between the ABS and GEN. Hence, the solid curve shows the upper limit of the GAX cycle. The dotted curve represents the results of the single-stage (or single-effect) NH_3/H_2O VAR cycle, which gives the lower limit of the GAX cycle if the heat is not perfectly coupled. A practical system is supposed to perform between these two limits. The dashed curve represents the average of these two limits, which is an expected estimation of the actual performance.

Fig. 15 shows a comparison of the performance of the NH_3/H_2O GAX cycle and the DE-VAR cycle with the NH_3/[bmim][BF_4] and NH_3/[emim][SCN] pairs at the condition of $T_{abs} = T_{con}$ = 21 °C, indicating applications at high-latitude areas. T_{eva} is set to −5 and 0 °C. The temperature of the driving heat is varied to investigate its influence.

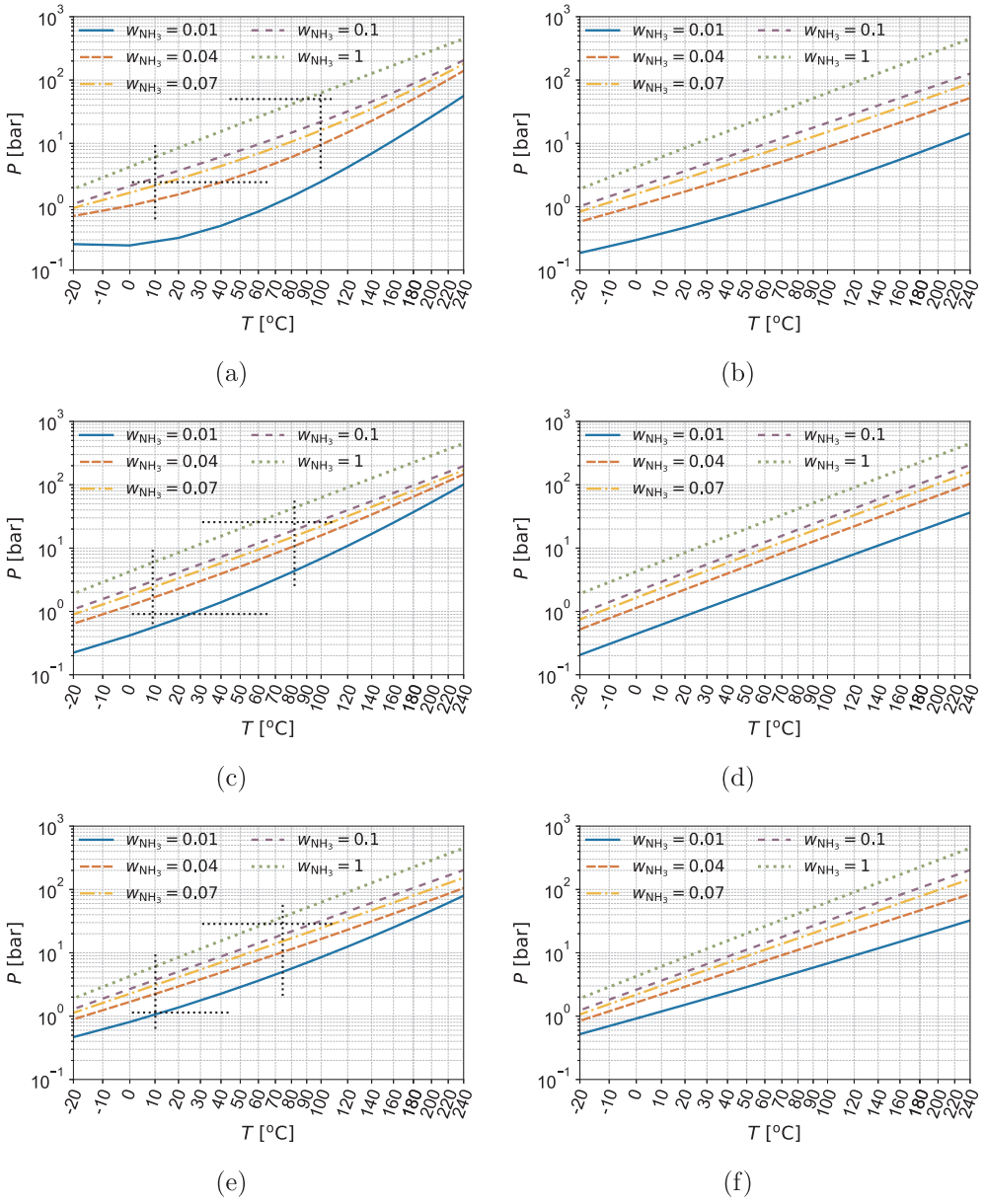

Fig. 11. Comparison of the vapor pressure curves generated only using the experimental VLE data (EXP) and the ones together using the experimental and simulated VLE data (SIM) for the studied NH_3/IL working pairs: (a) NH_3/[emim][SCN] pair (EXP [11]), (b) NH_3/[emim][SCN] pair (EXP [11] + SIM) (c) NH_3/[bmim][BF_4] pair (EXP [10]), (d) NH_3/[bmim][BF_4] pair (EXP [10] + SIM), (e) NH_3/[emim][Tf_2N] pair (EXP [10]), (f) NH_3/[emim][Tf_2N] pair (EXP [10] + SIM). Vertical and horizontal dashed lines represent temperature and pressure boundaries of EXP data.

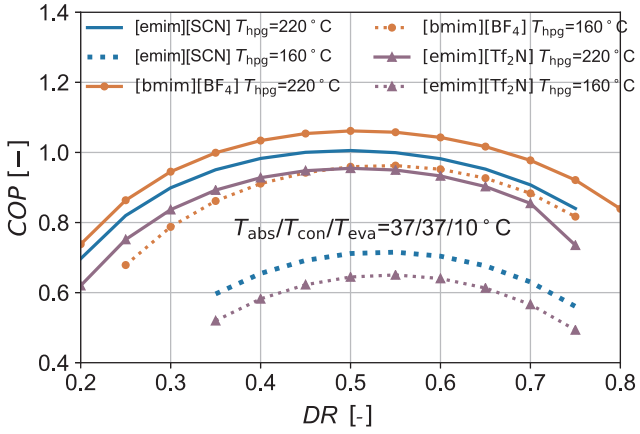

Fig. 12. Influence of the distribution ratio on the coefficient of performance of the DE-VAR with working pair NH_3/[emim][SCN], NH_3/[bmim][BF_4] and NH_3/[emim][Tf_2N]. The performance is calculated at the conditions T_{hpg} are 220 or 160 °C, and $T_{abs}/T_{con}/T_{eva}$ are kept constant at 37/37/10 °C.

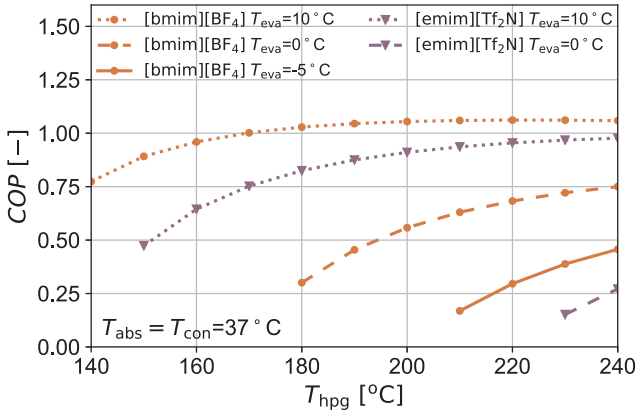

(a)

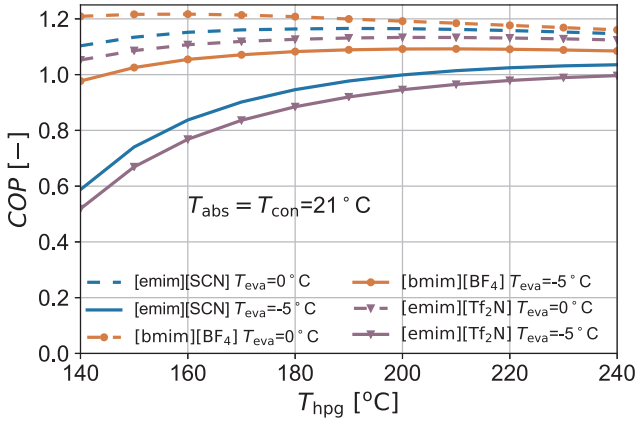

(b)

Fig. 13. Influence of the cooling temperature, T_{eva}, on the coefficient of performance of the DE-VAR with working pairs NH_3/[emim][SCN] (smooth curves), NH_3/[bmim][BF_4] (curves with round symbols) and NH_3/[emim][Tf_2N] (curves with triangle symbols) for applications in: (a) tropical areas (T_{con} = T_{abs} = 37 °C) and (b) high-latitude areas (T_{con} = T_{abs} = 21 °C).

Note that the performance of the GAX cycle is represented by the average value between the ideal GAX and normal SE-VAR performance. The data of T_{gen} above 170 ° are based on extrapolation.

As shown in Fig. 15, the GAX cycle is able to reach a high

Table 5
Comparison of the effect of different VLE properties sources for NH_3/[bmim][BF_4] on the DE-VAR cycle performance at the condition of $T_{hpg}/T_{abs}/T_{con}/T_{eva}$ = 240/37/37/-5 °C (*DR* = 0.5).

Relevant parameters		EXP [10] VLE (Fig. 11(c))	EXP [10] + SIM VLE (Fig. 11(d))
w_5	[–]	0.0387	0.0383
w_{11b}	[–]	0.0245	0.0290
w_9	[–]	0.0064	0.0285
w_{13}	[–]	0.0156	0.0287
f	[–]	42.49	101.72
specific $\dot{Q}_{eva}$	[kJ/kg]	1158.32	1158.32
specific $\dot{Q}_{hpg}$	[kJ/kg]	1204.01	1638.62
specific $\dot{W}_p$	[kJ/kg]	321.80	772.49
COP	[–]	0.759	0.480

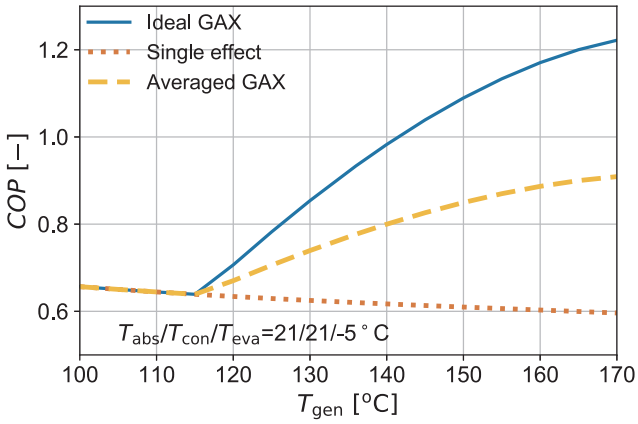

Fig. 14. Comparison of performance between the ideal NH_3/H_2O GAX cycle, the single-stage NH_3/H_2O cycle at various T_{gen} conditions ($T_{abs}/T_{con}/T_{eva}$ = 21/21/−5 °C). Solid curve indicates the "ideal" GAX performance and the dotted curve indicates the "degraded" GAX, i.e. the single-effect cycle. The dashed curve denotes the expected performance of a real system.

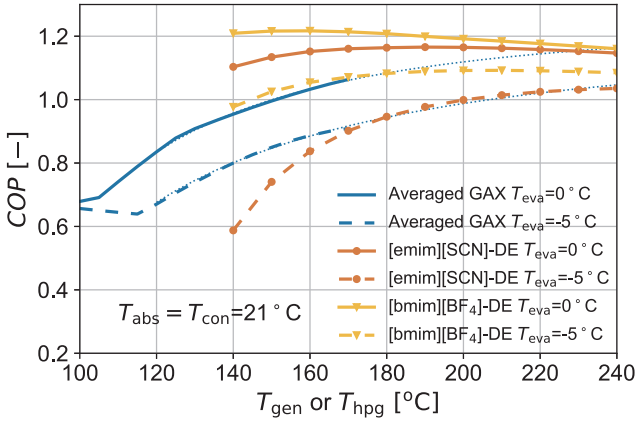

Fig. 15. Comparison of the performance of the DE-VAR with working pairs NH_3/[bmim][BF_4], NH_3/[emim][SCN] and the NH_3/H_2O GAX cycle at condition T_{abs} = T_{con} = 21 °C. Smooth curves indicate the GAX performance and the dotted curves are extrapolations of their trend lines. The solid curves denote the performance of cooling at T_{eva} = 0 °C and the dashed curves denote the performance of cooling at T_{eva} = −5 °C.

performance even when the driving temperature is relatively low. With the T_{gen} increasing, the performance of this cycle is increasing less rapidly. The DE-VAR with NH_3/[emim][SCN] pair shows a poor performance around 150 °C for a −5 °C cooling application. After a sharp initial increase, *COP* values of the DE-VAR increase only slightly when

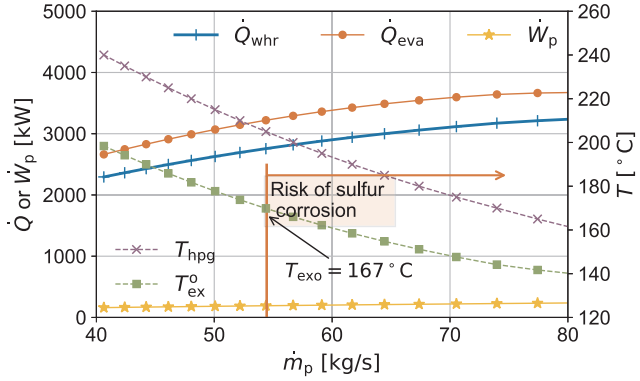

Fig. 16. The influence of the designed pump flow, $\dot{m}_p$, on operating parameters of the exhaust gas driven DE-VAR system with NH_3/[bmim][BF_4]. The case is based on a 90% diesel engine load, in high-latitude areas for a −5 °C cooling temperature. Note that for pump flows above 54.4 kg/s, the exhaust gas might condensate and cause sulfur corrosion.

T_{hpg} is above 180 °C. The *COP* value of the proposed cycle with NH_3/[bmim][BF_4] is approximately 10% higher than that of the averaged GAX cycle when they are driven by heat at 200 °C. In the higher temperature range, these two cycles show a similar performance. Considering the proposed DE-VAR applying ILs, there is no special need for a control strategy of the internal heat coupling, and the utilization of the ILs prevents the need for rectification of the refrigerant flow.

5.4. System integration of the double-effect vapor absorption cycle with the exhaust gas

Direct heat exchange is assumed between the exhaust gas and the strong NH_3/IL solution. DE-VAR cycles are designed for high temperature applications and a direct coupling could take full advantage of the high temperature exhaust gas. Thus, the waste heat recovery (WHR) exchanger, i.e. the flue gas cooler, also plays the role of a high pressure generator.

5.4.1. Recoverable heat and corresponding cooling capacities

For the exhaust gas stream associated with the WHR heat exchanger applied in typical modes, the inlet temperature, T^i_{ex}, and the flow rate, $\dot{m}_{ex}$, are listed in Table 3. The outlet temperature, T^o_{ex}, cannot be cooled down below 167 °C to prevent the risk of sulfur corrosion [4]. With these constraints, the driving heat of the DE-VAR system is the recovered heat from the exhaust gas, $\dot{Q}_{whr}$, which is expressed as,

$$\dot{Q}_{whr} = c_p^{ex}\dot{m}_{ex}(T^i_{ex} - T^o_{ex}) \quad (13)$$

where the specific heat of the exhaust gas, c_p^{ex}, is taken as 1.08 kJ/(kg K) [46].

In the design phase, a pinch temperature of 10 K is assumed in this HX. T_8 cannot be below 157 °C to prevent corrosion problems. The value of T_8 is also influenced by the operation of the cycle. Hence, the pumping flow, which is easy to adjust by changing the pump settings, is studied to explore its influence on the cooling capacity and on the heat recycling performance.

Fig. 16 depicts a case in which the inlet exhaust gas stream is at 340 °C and 15 kg/s (which corresponds to the majority of the operating cases: Mode 1 and 2 in Table 3), in high-latitude areas ($T_{abs} = T_{con} = 21$ °C) and for a $T_{eva} = -5$ °C cooling application.

In the proposed DE-VAR, a higher driving temperature leads to a higher T_8. To maintain a fixed temperature difference of heat transfer, a higher T^o_{ex} is required. Accordingly, the exhaust gas has a smaller temperature range over which it can be cooled and a smaller waste heat can be recovered. While a higher driving temperature also results in a higher *COP*. These dependencies influence the cooling capacity $\dot{Q}_{eva}$ (round symbols), and lead to an initial increase, and then to a constant value as a function of the pump flow.

However for the studied case, when the pump flow of the solution, $\dot{m}_p$, is higher than 54.4 kg/s, the exhaust gas cannot be cooled below 167 °C as shown in Fig. 16. Even though cooling and heat recovery performances are better in this range, the DE-VAR system cannot be operated due to the risk of sulfur corrosion. Therefore, the optimum performance is achieved at a pump flow of 54.4 kg/s. The corresponding cooling capacity is 3220 kW.

Table 6 summarizes the operating parameters and optimum cooling performance when using the DE-VAR with the studied three working fluids for different engine loads.

The exhaust gas driven DE-VAR system with NH_3/[bmim][BF_4] working pair is always larger than 1518 kW in the high-latitude environment, which has the largest cooling capacity among the three studied working pairs. And for an engine load of 90%, the cooling capacity is able to reach 3220 kW. It has the potential to substitute at least one of the RSW plants in the studied fishing vessel (Table 2) for most of the operating condition. The solution pump flow, $\dot{m}_p$, of the NH_3/[bmim][BF_4] working pair is also lower than the ones of the other two pairs.

5.4.2. State information

The state point information for the working fluid, NH_3/[bmim][BF_4] in the DE-VAR system, is listed in Table 7, for the above studied case in a condition of $T_{hpg}/T_{abs}/T_{con}/T_{eva} = 205/21/21/-5$ °C.

Due to the pressure drop in the valve and heating in the SHXs, solutions at state points 7c and 8 may have NH_3 vapor generated [16]. A close investigation reveals that only small amounts of NH_3 vapor are generated before entering the generators. Results of NH_3 fractions and specific enthalpies of these two points in Table 7 are the data for bulk

Table 6
The optimum cooling performance ($\dot{Q}_{eva}$), corresponding recovered waste heat ($\dot{Q}_{whr}$), DE-VAR cycle performance (*f* and *COP*, $\dot{m}_p$, and $\dot{W}_p$), and operating conditions (T^i_{ex}, T^o_{ex}, T_8, and T_{hpg}) for different diesel engine loads with the working pair NH_3/[emim][SCN], NH_3/[bmim][BF_4], and NH_3/[emim][Tf_2N] in high latitude areas.

	NH_3/[emim][SCN]			NH_3/[bmim][BF_4]			NH_3/[emim][Tf_2N]		
Engine load	90%	70%	40%	90%	70%	40%	90%	70%	40%
T^i_{ex} [°C]	340	326.5	307.4	340	326.5	307.4	340	326.5	307.4
T^o_{ex} [°C]	170.4	170.4	170.4	169.8	169.8	169.8	179.6	179.6	179.6
T_8 [°C]	160.4	160.4	160.4	159.8	159.8	159.8	169.6	169.6	169.6
T_{hpg} [°C]	190	190	190	205	205	205	200	200	200
f [–]	28.7	28.7	28.7	20.4	20.4	20.4	22.8	22.8	22.8
COP [–]	0.977	0.977	0.977	1.092	1.092	1.092	0.946	0.946	0.946
$\dot{m}_p$ [kg/s]	69.8	51.4	32.9	54.4	40.1	25.6	94.5	69.2	43.9
$\dot{W}_p$ [kW]	257	189	121	191	141	90	257	188	120
$\dot{Q}_{whr}$ [kW]	2748	2023	1295	2756	2030	1300	2599	1904	1208
$\dot{Q}_{eva}$ [kW]	2936	2162	1383	3220	2372	1518	2701	1979	1255

Table 7
State points of the DE-VAR at a condition of $T_{hpg}/T_{abs}/T_{con}/T_{eva}$ = 205/21/21/-5°C) with the working fluid pair of NH_3/[bmim][BF_4] (DR = 0.5, $\dot{m}_p$ = 54.4 kg/s).

Point	ṁ [kg/s]	T [°C]	P [bar]	w_{NH_3} [–]	h^* [kJ/kg]
1	2.67	10.6	8.85	1	146.90
2	2.67	−5.0	3.55	1	146.90
3	2.67	−5.0	3.55	1	1353.86
4	2.67	14.5	3.55	1	1402.69
5	54.40	21.0	3.55	0.0766	79.38
6	54.40	21.0	39.53	0.0766	82.37
7	54.40	57.2	39.53	0.0766	148.41
7a	27.20	57.2	39.53	0.0766	148.41
7b	27.20	57.2	39.53	0.0766	148.41
7c**	27.20	57.2	8.85	0.0766	148.41
8**	27.20	159.8	39.53	0.0766	393.02
9	25.57	205.0	39.53	0.0179	411.84
10	25.57	67.2	39.53	0.0179	151.64
11	51.73	70.1	8.85	0.0290	160.09
11a	25.57	67.2	8.85	0.0179	151.64
11b	26.16	72.9	8.85	0.0399	168.34
12	51.73	31.0	8.85	0.0290	90.64
13	51.73	31.0	3.55	0.0290	90.64
14	1.63	205.0	39.53	1	1791.27
15	1.63	77.9	39.53	1	485.50
16	1.63	21.0	8.85	1	485.50
17	1.04	72.9	8.85	1	1517.54
18	2.67	21.0	8.85	1	195.73

* Specific enthalpies are calculated based on an arbitrarily chosen reference state of T = −23 °C and P = 10 bar.

** At state points 7c and 8, the NH_3 may boil off from the solution. Saturated fractions and qualities of state points 7c and 8 are: w_{sat}^{7c} = 0.0672, q_{7c} = 0.01. w_{sat}^{8} = 0.0384, q_8 = 0.04.

streams (saturated solution with NH_3 vapor). Specific enthalpies of the bulk stream are obtained via,

$$h^{sol}(T, P, w_{NH_3}) = (1-q)h_{sat}^{sol} + qh^{V} \quad (14)$$

where h_{sat}^{sol} and h^V are the specific enthalpies for the saturated solution part and the vapor part, respectively. q is the quality, which is identified as,

$$q = \frac{w-w_{sat}}{1-w_{sat}} \quad (15)$$

The qualities and saturated NH_3 fractions of these two points are additionally listed in the footnote of Table 7.

5.5. Feasibility consideration

The above studied IL-based working pairs show a promising technical performance in the DE-VAR at high-temperature applications. Before implementing the cycle, thermal stabilities of the investigated ILs and the potential economic benefits must be considered.

5.5.1. Thermal stabilities

It has been reported that imidazolium ILs have high thermal stabilities [47]. The short and long-term thermal stabilities of [emim][SCN] have been studied by Navarro et al. [34]. Liu et al. [48] investigated short and long-term thermal stability of [bmim][BF_4]. Feng et al. [49] also carried out thermal analysis of [bmim][BF_4]. Heym et al. [50] measured the thermal decomposition of [emim][Tf_2N]. The work of Villanueva et al. [51] included the long-term stabilities of [emim][Tf_2N]. The key findings of these studies are summarized in Table 8.

It can be seen that the thermal stability of [bmim][BF_4] and [emim][Tf_2N] is better than that of [emim][SCN] regarding both short and long-term stability. The two ILs have also been classified into the group of "most stable" ILs by Cao and Mu [47]. The conducted long-term tests have shown the applicability of [bmim][BF_4] below 250 °C. [emim][SCN] has shown obvious mass loss above 160 °C and for this reason it cannot be applied in DE-VAR systems.

5.5.2. Economic and environmental benefits

It can be concluded that the proposed DE-VAR system with NH_3/[bmim][BF_4] is promising for the application in high-latitude areas. An accurate estimation of the initial cost and the system size relies on a thorough understanding of the heat and mass transfer of the newly-proposed working fluids and further investigation is required. Nevertheless, the operational cost can be estimated based on the analysis in this study. Table 9 shows the two options of replacing RSW plants with the proposed exhaust gas driven DE-VAR system.

The first option is to replace one RSW plant. The exhaust gas for all 5 engine operating modes (Mode 1–5 shown in Table 3) is able to drive the proposed DE-VAR system to produce the equivalent cooling capacity of one RSW. For these operating time (7320 h per year), a saved primary energy can be obtained via the difference in power consumption of the proposed system and the existing compression one, which is 4.77 TJ/year. If the CO_2 emission of diesel oil is taken as 778 g/kWh_e (diesel) [52], the CO_2 emission during fishing can be reduced by 1031 tons/year. Option 2 concerns replacing two RSW plants with one DE-VAR system, while this option is able to provide an equivalent cooling capacity of two RSW plants only when the engine operates at a 90% load. For this case, by operating it 5800 h/year, the saved energy is 7.33 TJ/year and the corresponding reduced CO_2 emission is 1633.5 tons/year.

6. Conclusions

A waste heat recovery cooling system is proposed which uses ammonia/ionic liquid mixtures as working fluids in a double-effect vapor absorption refrigeration (DE-VAR) system. A multi-scale analysis is carried out to study its performance in a fishing vessel. The analysis includes Monte Carlo simulation to predict vapor-liquid equilibria at high temperatures and pressures, thermodynamic modeling for cooling cycle analysis, and system evaluation when integrated with engine exhaust gas. Based on the work, the following conclusions could be drawn:

Table 8
A summary of assessment for the thermal stabilities of the studied ILs [34,48–51].

	[emim][SCN] [34]	[bmim][BF_4]	[emim][Tf_2N]
T_{onset}*	525.5 (5 K/min) 538.6 (10 K/min) 553.7 (20 K/min)	630 K (10 K/min) [48]	692 K (10 K/min) [50]
Long-term stability	Obvious mass loss observed at and above 433.2 K during 48 h. No obvious mass loss observed at and below 393.2 K during 48 h.	It does not show an obvious mass loss at 513 K for 5 h [48]. Mass losses rates are 1.30% and 2.60% for 453 K and 573 K respectively, for 10 h. No obvious change for the Fourier Transform Infrared Spectroscopy analysis [49].	Mass losses rates are below 2% for 533 K for 5 h [51].

* T_{onset} is an extrapolated and reproducible temperature that denotes a point at which the weight loss begins. A graphic explanation can be found in literature, for instance, Navarro et al. [34].

Table 9
Economic and environmental benefits of replacing refrigeration seawater plants with the proposed system applied in high-latitude areas.

	In substitute of	Operating hours [hrs/year]	Saved energy [TJ/year]	Reduced CO_2 [tons/year]
Option 1	RSW × 1	7320	4.77	1030.8
Option 2	RSW × 2	5800	7.56	1633.5

- Monte Carlo simulations are capable to extend the vapor–liquid equilibrium data of the working fluids. The inclusion of the computed solubilities improves the quality of the extension of the NRTL model to high temperature and pressure conditions in comparison to solely using experimental data obtained at low temperatures and pressures.
- The ranking of the coefficient of performance (*COP*) for the three studied ILs within NH_3-based DE-VAR cycle is: [bmim][BF_4] > [emim][SCN] > [emim][Tf_2N]. The best IL candidate achieves a *COP* above 1.1 for −5 °C cooling in a fishing vessel operating in high-latitude areas.
- DE-VAR cycles show approximately 10% higher performance than GAX cycles with NH_3/H_2O for applications with high temperature driving heat.
- Because of stability problems at high temperatures, [emim][SCN] is not suitable for high-temperature applications of a double-effect vapor absorption refrigeration cycle.
- The proposed system with NH_3/[bmim][BF_4] can provide the cooling capacity of one refrigeration seawater (RSW) plant for all operating modes of the diesel engine, when driven by its exhaust gas (*COP* of 1.1, cooling capacity of 1518 kW). Thereby, 4.8 TJ of energy can be saved and 1030 tons of CO_2 emission can be avoided annually per fishing vessel. Alternatively, the proposed system can provide the cooling capacity of two RSW plants for most of the operating modes (cooling capacity of 3200 kW). Annually saved energy and reduced CO_2 emissions are 7.6 TJ and 1635 tons, respectively.

Acknowledgment

The authors would like to acknowledge the financial support from the China Scholarship Council (Scholarship 201406320184). We acknowledge support from the NWO Exacte Wetenschappen (Physical Sciences) for the use of supercomputer facilities, with financial support from the Nederlandse Organisatie voor Wetenschappelijk Onderzoek (Netherlands Organization for Scientific Research, NWO). TJHV acknowledges NWO-CW (Chemical Sciences) for a VICI grant. The authors also thank Mr. Yunxiang Wu for refining Figs. 4, 7 and 8.

Appendix A. Thermophysical properties diagrams of the studied working fluids

Based on the thermal properties methods discussed in Section 2, the ln *P*-(-1/*T*) and *h*-*w* diagrams of the studied working fluids can be provided. Note that the properties described in these diagrams apply for saturated-liquid conditions.

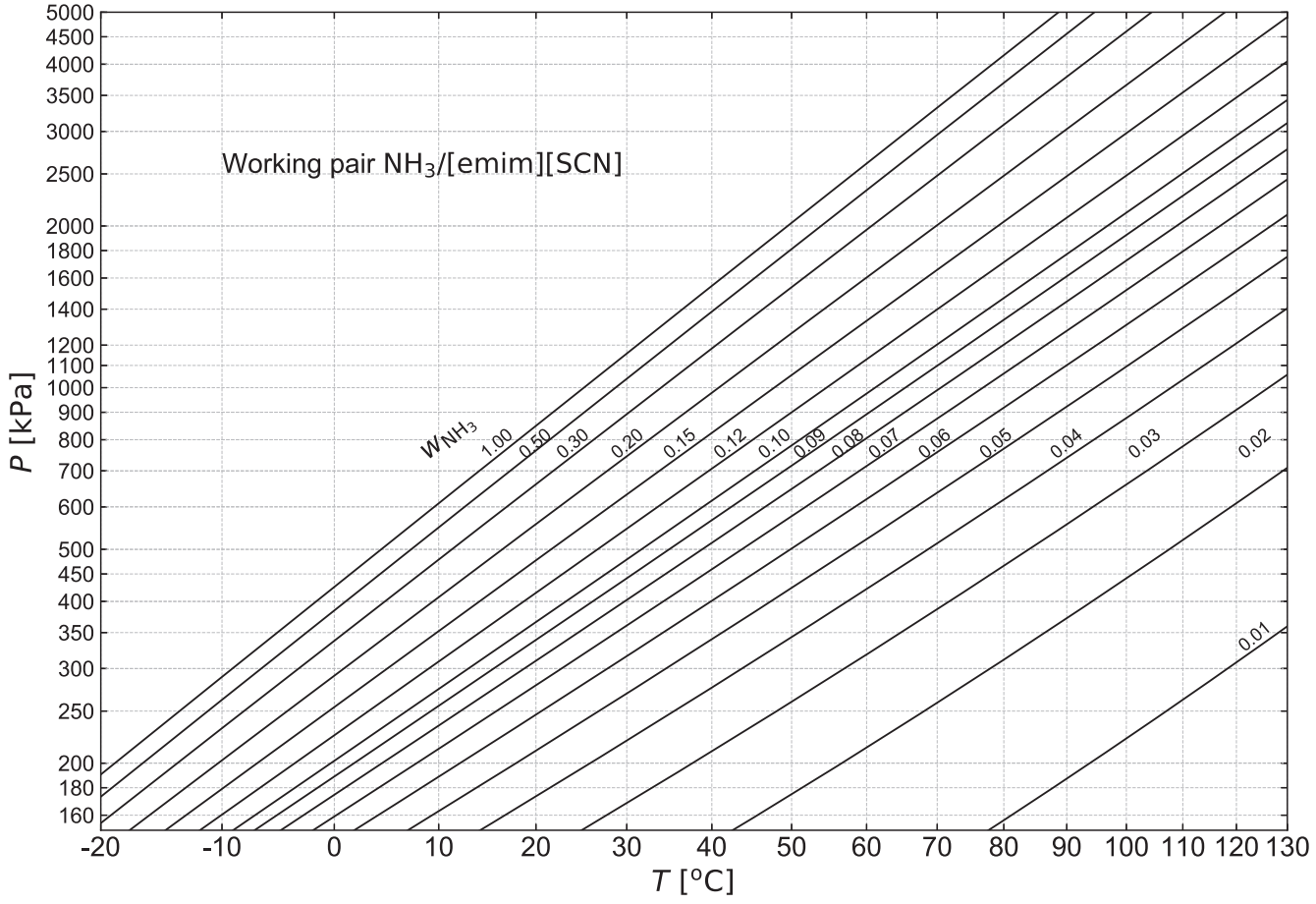

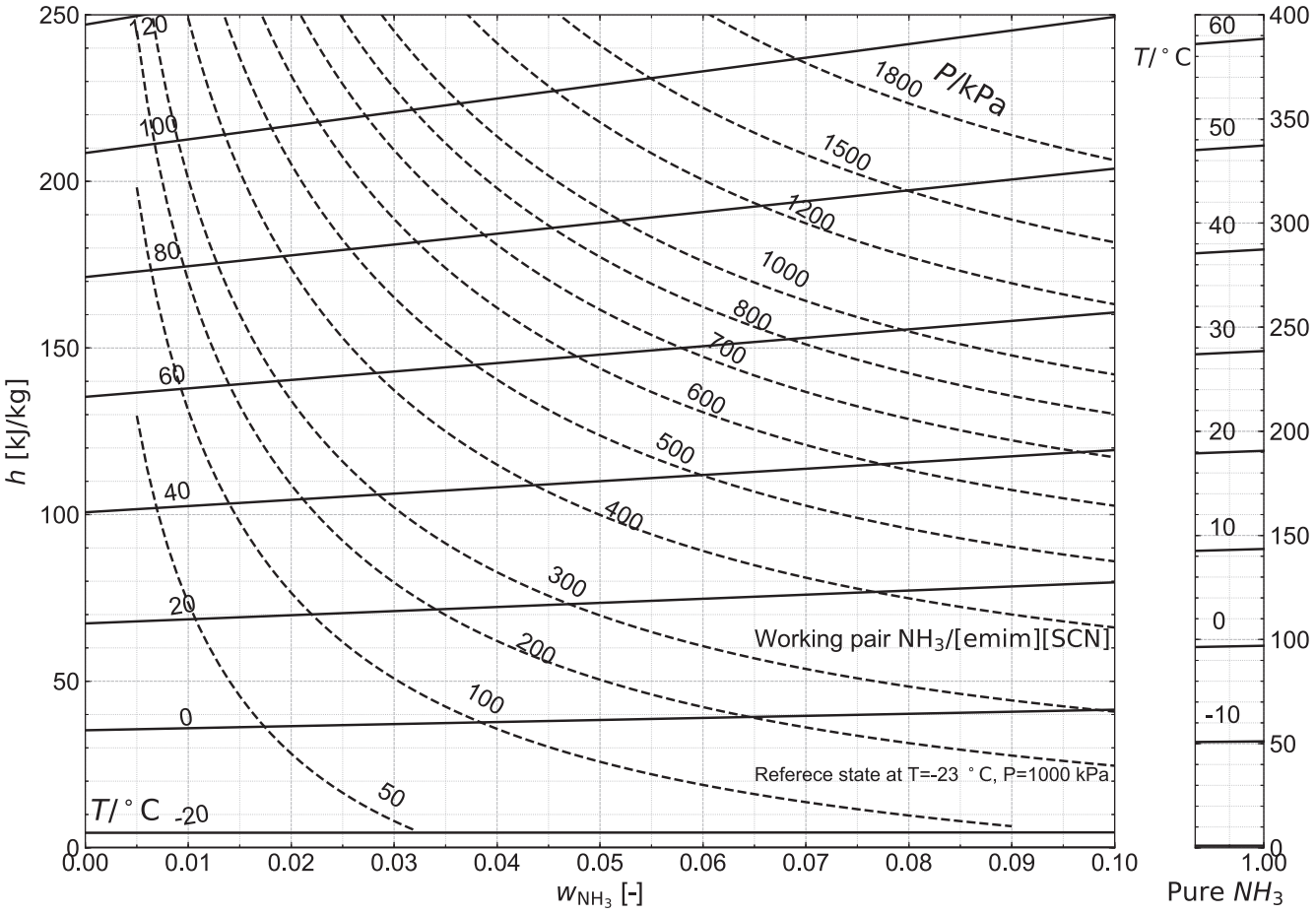
h [kJ/kg]
w_{NH_3} [-]
T/ ° C
P/kPa
Working pair NH3/[emim][SCN]
Referece state at T=-23 ° C, P=1000 kPa
Pure NH_3

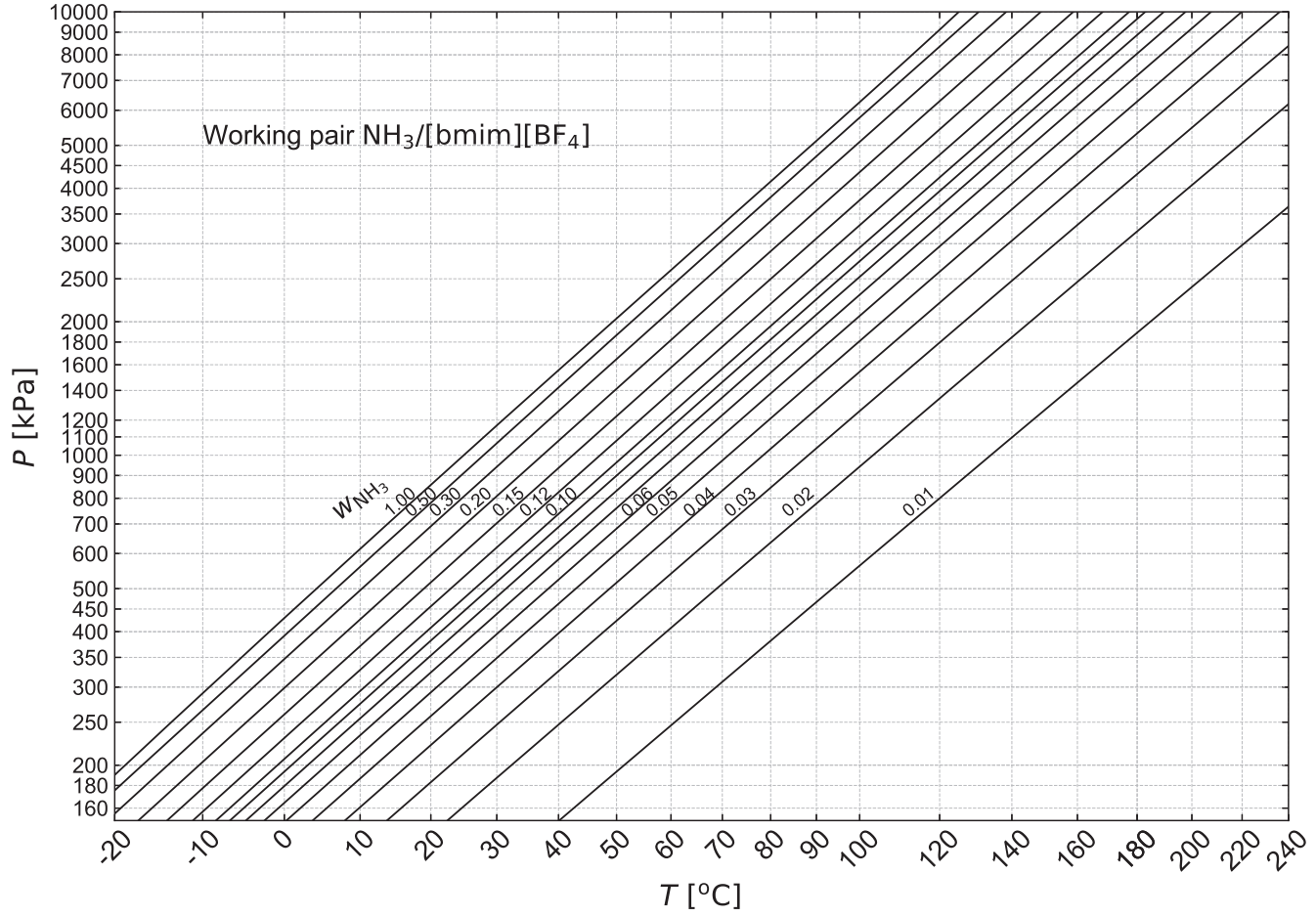
Working pair NH3/[bmim][BF4]
P [kPa]
T [°C]
wNH3
1.00
0.50
0.30
0.20
0.15
0.12
0.10
0.06
0.05
0.04
0.03
0.02
0.01

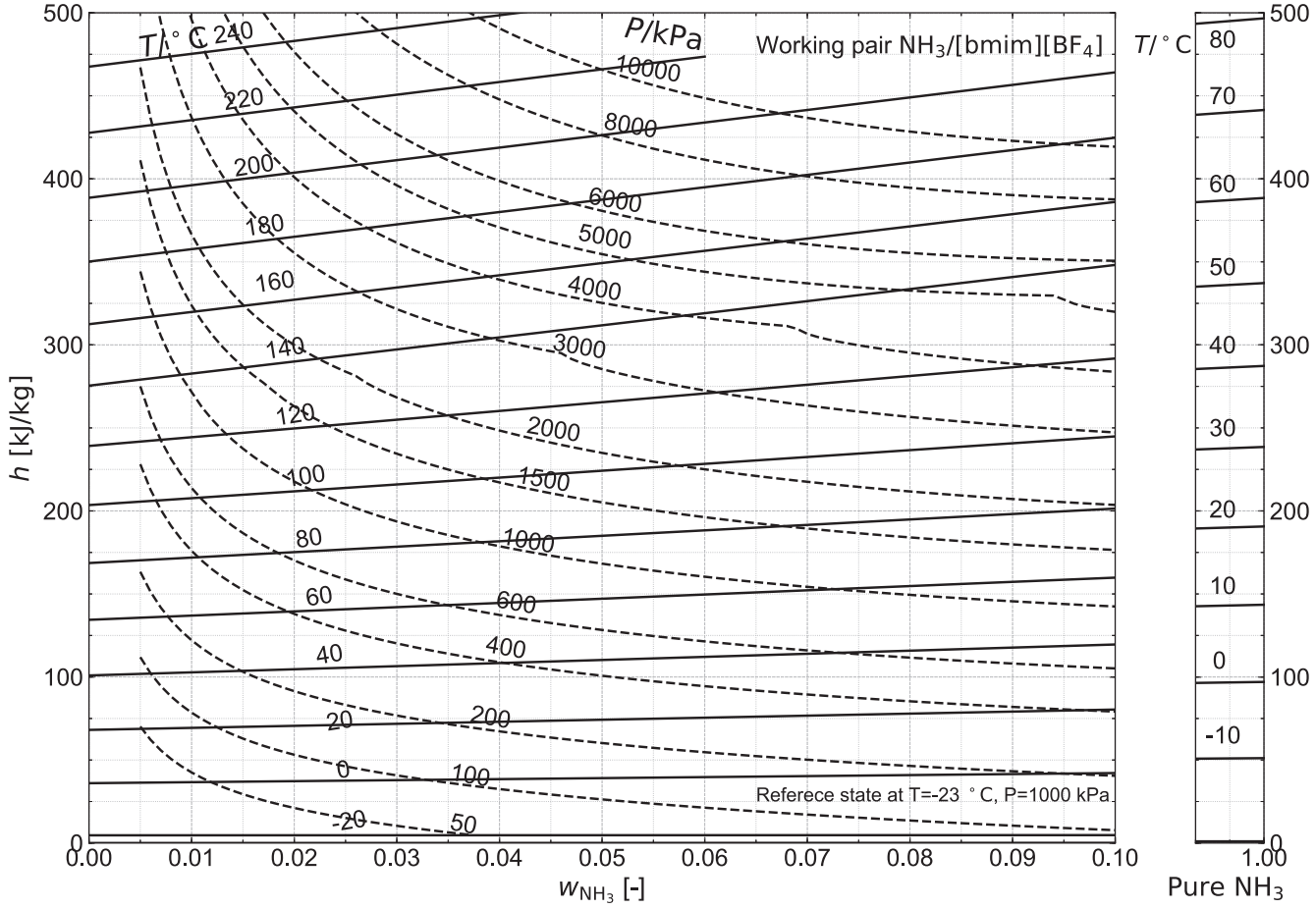
T/° C
P/kPa
Working pair NH3/[bmim][BF4]
T/° C
h [kJ/kg]
wNH3 [-]
Pure NH3
Referece state at T=-23 ° C, P=1000 kPa
240
220
200
180
160
140
120
100
80
60
40
20
0
-20
10000
8000
6000
5000
4000
3000
2000
1500
1000
600
400
200
100
50
80
70
60
50
40
30
20
10
0
-10
0.00
0.01
0.02
0.03
0.04
0.05
0.06
0.07
0.08
0.09
0.10
1.00
0
100
200
300
400
500

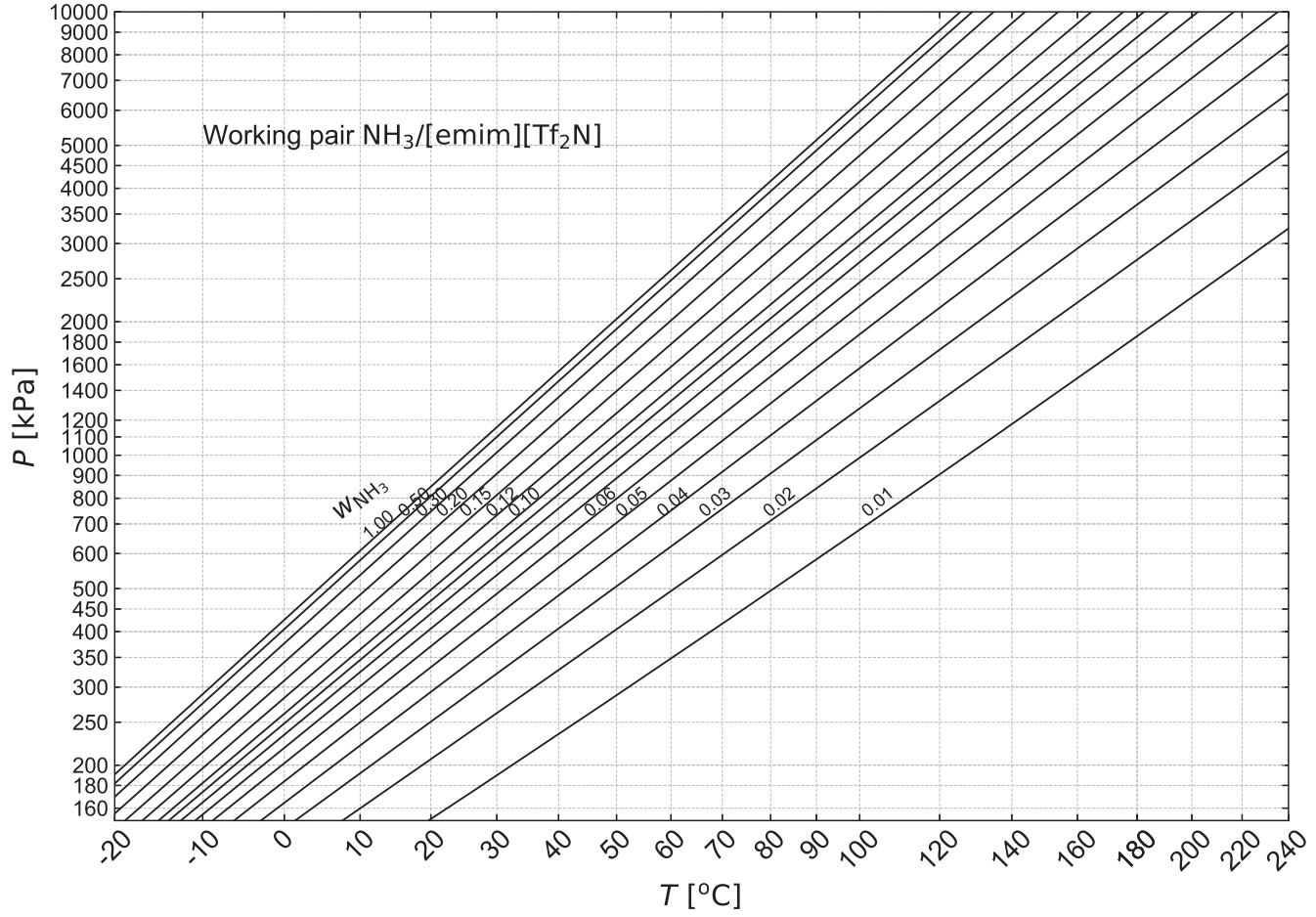
Working pair NH3/[emim][Tf2N]
P [kPa]
T [°C]
wNH3
1.00
0.50
0.30
0.20
0.15
0.12
0.10
0.06
0.05
0.04
0.03
0.02
0.01

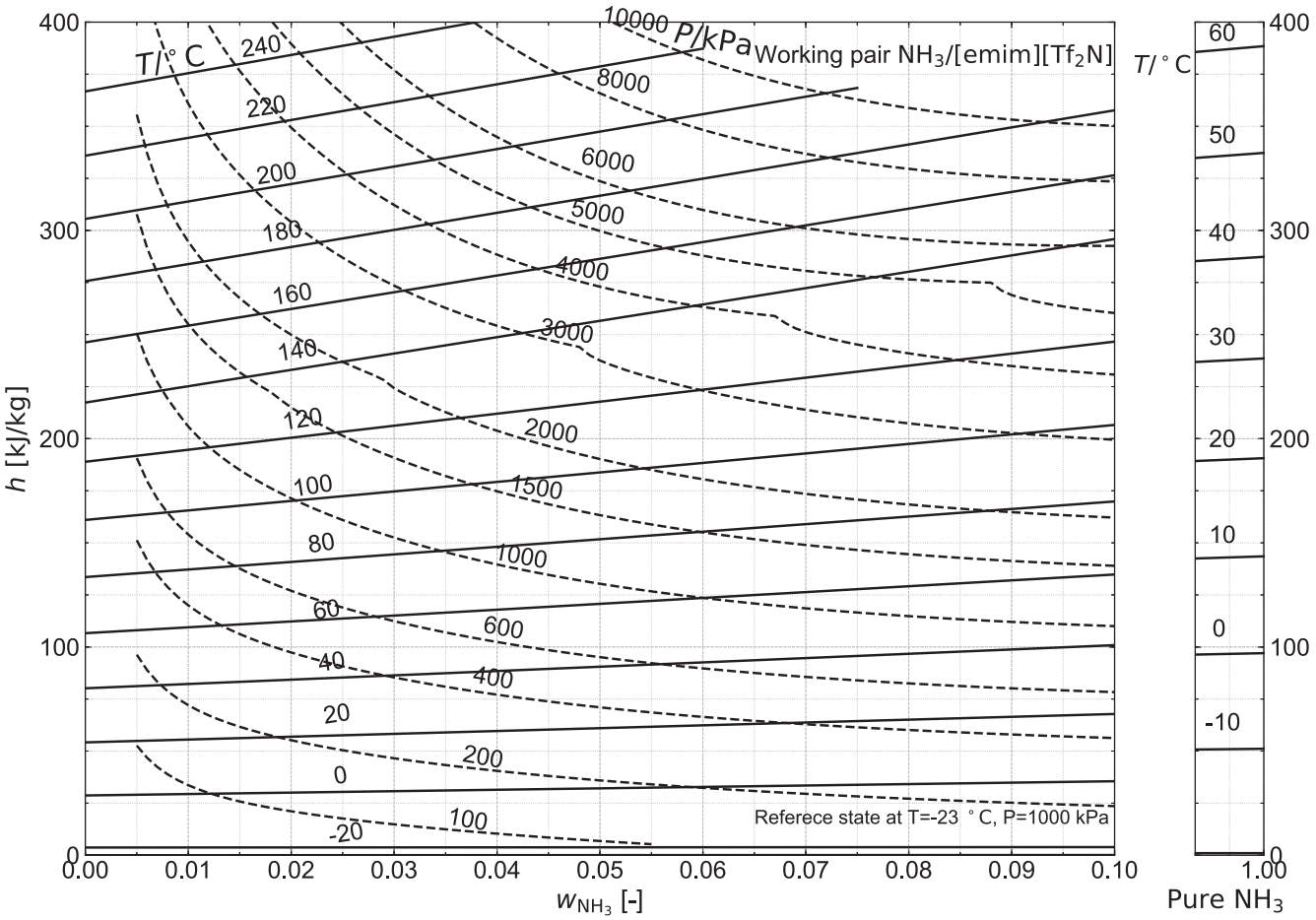

Appendix B. Supplementary material

Supplementary data associated with this article can be found, in the online version, at https://doi.org/10.1016/j.enconman.2018.08.060.

References

[1] International Maritime Organization, Third IMO Greenhouse Gas Study 2014, Tech. Rep., IMO, London, URL http://www.imo.org/en/OurWork/Environment/PollutionPrevention/AirPollution/Documents/Third%20Greenhouse%20Gas%20Study/GHG3%20Executive%20Summary%20and%20Report.pdf; 2014 [Accessed 28 November 2017].

[2] Shu G, Liang Y, Wei H, Tian H, Zhao J, Liu L. A review of waste heat recovery on two-stroke IC engine aboard ships. Renew Sustain Energy Rev 2013;19:385–401.

[3] Ruiz V. Analysis of existing refrigeration plants onboard fishing vessels and improvement possibilities. In: Second International Symposium on Fishing Vessel Energy Efficiency, Vigo, Spain; 2012.

[4] Salmi W, Vanttola J, Elg M, Kuosa M, Lahdelma R. Using waste heat of ship as energy source for an absorption refrigeration system. Appl Therm Eng 2017;115:501–16.

[5] MAN Diesel & Turbon LTD, Thermo Efficiency System for Reduction of Fuel Consumption and CO_2 Emission, Tech. Rep., Copenhagen, URL http://marine.man.eu/docs/librariesprovider6/technical-papers/thermo-efficiency-system.pdf?sfvrsn=22; 2014 [Accessed 28 November 2017].

[6] Fernández-Seara J, Vales A, Vázquez M. Heat recovery system to power an onboard NH_3-H_2O absorption refrigeration plant in trawler chiller fishing vessels. Appl Therm Eng 1998;18(12):1189–205.

[7] Cao T, Lee H, Hwang Y, Radermacher R, Chun HH. Performance investigation of engine waste heat powered absorption cycle cooling system for shipboard applications. Appl Therm Eng 2015;90:820–30.

[8] Herold K, Radermacher R, Klein S. Absorption Chillers and Heat Pumps, Second Edition. CRC Press, ISBN 978-1498714341; 2016.

[9] Zheng D, Dong L, Huang W, Wu X, Nie N. A review of imidazolium ionic liquids research and development towards working pair of absorption cycle. Renew Sustain Energy Rev 2014;37:47–68.

[10] Yokozeki A, Shiflett MB. Ammonia solubilities in room-temperature ionic liquids. Ind Eng Chem Res 2007;46(5):1605–10.

[11] Yokozeki A, Shiflett MB. Vapor-liquid equilibria of ammonia + ionic liquid mixtures. Appl Energy 2007;84(12):1258–73.

[12] Chen W, Liang S, Guo Y, Gui X, Tang D. Investigation on vapor-liquid equilibria for binary systems of metal ion-containing ionic liquid [bmim]Zn_2Cl_5/NH_3 by experiment and modified UNIFAC model. Fluid Phase Equilib 2013;360:1–6.

[13] Chen W, Liang S, Guo Y, Tang D. Thermodynamic analysis of an absorption system using [bmim]Zn_2Cl_5/NH_3 as the working pair. Energy Convers Manage 2014;85:13–9.

[14] Ruiz E, Ferro VR, De Riva J, Moreno D, Palomar J. Evaluation of ionic liquids as absorbents for ammonia absorption refrigeration cycles using COSMO-based process simulations. Appl Energy 2014;123:281–91.

[15] Cera-Manjarres A. Experimental determination and modelling of thermophysical properties of ammonia/ionic liquid mixtures for absorption refrigeration systems. Ph.D. thesis. Universitat Rovira I Virgili; 2015.

[16] Wang M, Infante Ferreira CA. Absorption heat pump cycles with NH_3 – ionic liquid working pairs. Appl Energy 2017;204:819–30.

[17] Wang M, Infante Ferreira CA. Performance analysis of double-effect absorption heat pump cycle using NH_3/ILs pairs. In: Proc of the 12th IEA Heat Pump Conference, Rotterdam, NL; 2017b.

[18] Schouten B. Advanced NH_3 based absorption refrigeration cycles: Modelling of the ionic liquid based double-effect cycles. Master's thesis. Delft University of Technology; 2017.

[19] Becker TM, Wang M, Kabra A, Jamali SH, Ramdin M, Dubbeldam D, Infante Ferreira CA, Vlugt TJH, et al. Absorption refrigeration cycles with ammonia-ionic liquid working pairs studied by molecular simulation. Ind Eng Chem Res 2018;57(15):5442–52.

[20] Frenkel D, Smit B. Understanding molecular simulation: from algorithms to applications. Academic Press; 2001. ISBN 978-0122673511.

[21] Allen MP, Tildesley DJ. Computer Simulation of Liquids. Oxford University Press; 2017.

[22] Liu H, Maginn E. A molecular dynamics investigation of the structural and dynamic properties of the ionic liquid 1-n-butyl-3-methylimidazolium bis(trifluoromethanesulfonyl)imide. J Chem Phys 2011;135(12):124507.

[23] Ramdin M, Balaji SP, Vicent-Luna JM, Gutiérrez-Sevillano JJ, Calero S, de Loos TW, Vlugt TJH. Solubility of the precombustion gases CO_2, CH_4, CO, H_2, N_2, and H_2S in

the ionic liquid [bmim][Tf_2N] from Monte Carlo simulations. J Phys Chem C 2014;118(41):23599–604.
[24] Shi W, Maginn EJ. Continuous fractional component Monte Carlo: an adaptive biasing method for open system atomistic simulations. J Chem Theor Comput 2007;3(4):1451–63.
[25] Tenney CM, Massel M, Mayes JM, Sen M, Brennecke JF, Maginn EJ. A computational and experimental study of the heat transfer properties of nine different ionic liquids. J Chem Eng Data 2014;59(2):391–9.
[26] Liu H, Maginn E, Visser AE, Bridges NJ, Fox EB. Thermal and transport properties of six ionic liquids: an experimental and molecular dynamics study. Ind Eng Chem Res 2012;51(21):7242–54.
[27] Canongia Lopes JN, Pádua AA. Molecular force field for ionic liquids III: Imidazolium, pyridinium, and phosphonium cations; chloride, bromide, and dicyanamide anions. J Phys Chem B 2006;110(39):19586–92.
[28] Zhang L, Siepmann JI. Development of the TraPPE force field for ammonia. Collect Czech Chem Commun 2010;75(5):577–91.
[29] Dubbeldam D, Calero S, Ellis DE, Snurr RQ. RASPA: molecular simulation software for adsorption and diffusion in flexible nanoporous materials. Mol Simul 2016;42(2):81–101.
[30] Wang M, Becker TM, Infante Ferreira CA. Assessment of vapor-liquid equilibrium models for ionic liquid based working pairs in absorption cycles. Int J Refrig 2018;87:10–25.
[31] Matkowska D, Hofman T. High-pressure volumetric properties of ionic liquids: 1-butyl-3-methylimidazolium tetrafluoroborate, [C_4mim][BF_4], 1-butyl-3-methylimidazolium methylsulfate [C_4mim][$MeSO_4$] and 1-ethyl-3-methylimidazolium ethylsulfate, [C_2mim][$EtSO_4$]. J Mol Liq 2012;165:161–7.
[32] Ficke LE, Novak RR, Brennecke JF. Thermodynamic and thermophysical properties of ionic liquid + water systems. J Chem Eng Data 2010;55(11):4946–50.
[33] Tariq M, Serro AP, Mata JL, Saramago B, Esperança JM, Lopes JN, et al. High-temperature surface tension and density measurements of 1-alkyl-3-methylimidazolium bistriflamide ionic liquids. Fluid Phase Equilib 2010;294(1-2):131–8.
[34] Navarro P, Larriba M, Rojo E, García J, Rodríguez F. Thermal properties cyano-based ionic liquids. J Chem Eng Data 2013;58(8):2187–93.
[35] Paulechka YU, Blokhin AV, Kabo GJ. Evaluation of thermodynamic properties for non-crystallizable ionic liquids. Thermochim Acta 2015;604:122–8.
[36] Nieto de Castro CA, Lourenco MJV, Ribeiro APC, Langa E, Vieira SIC, Goodrich P, et al. Thermal properties of ionic liquids and ionanofluids of imidazolium and pyrrolidinium liquids. J Chem Eng Data 2010;55(2):653–61.
[37] Paulechka YU, Blokhin AV, Kabo GJ, Strechan AA. Thermodynamic properties and polymorphism of 1-alkyl-3-methylimidazolium bis(triflamides). J Chem Thermodyn 2007;39(6):866–77.
[38] Ferreira AF, Simões PN, Ferreira AG. Quaternary phosphonium-based ionic liquids: thermal stability and heat capacity of the liquid phase. J Chem Thermodyn 2012;45(1):16–27.
[39] Dong L, Zheng D, Nie N, Li Y. Performance prediction of absorption refrigeration cycle based on the measurements of vapor pressure and heat capacity of H_2O + [DMIM]DMP system. Appl Energy 2012;98:326–32.
[40] Lemmon EW, Huber ML, McLinden MO. NIST reference fluid thermodynamic and transport properties-REFPROP; 2013.
[41] Vasilescu C, Infante Ferreira CA. Solar driven multi-effect sub-zero ammonia based sorption cycles. In: Proceedings of the international sorption heat pump conference (ISHPC11), Padua; 2011. p. 885–892.
[42] Wärtsilä, Wärtsilä 38 Project Guide. Tech. Rep. Wärtsilä Ship Power Technology, URL http://www.dieselduck.info/machine/01%20prime%20movers/Wartsila%2038%20project%20guide.pdf 2008, [Accessed 24 November 2017].
[43] Poling BE, Prausnitz JM, O'Connell JP. The properties of gases and liquids. McGraw-Hill; 2001. ISBN 9780070116825.
[44] Arun M, Maiya M, Murthy S. Performance comparison of double-effect parallel-flow and series flow water-lithium bromide absorption systems. Appl Therm Eng 2001;21(12):1273–9.
[45] Vasilescu C, Infante Ferreira CA. Solar driven double-effect absorption cycles for sub-zero temperatures. Int J Refrig 2014;39:86–94.
[46] Petrecca G. Industrial energy management: principles and applications. Springer; 2012. ISBN 978-1-4615-3160-9.
[47] Cao Y, Mu T. Comprehensive investigation on the thermal stability of 66 ionic liquids by thermogravimetric analysis. Ind Eng Chem Res 2014;53(20):8651–64.
[48] Liu P, Wang M, Cheng Z-M. Thermal stability and vapor liquid equilibrium for imidazolium ionic liquids as alternative reaction media. J Chem Eng Data 2015;60(3):836–44.
[49] Feng W-q, Lu Y-h, Chen Y, Lu Y-w, Yang T. Thermal stability of imidazolium-based ionic liquids investigated by TG and FTIR techniques. J Therm Anal Calorim 2016;125(1):143–54.
[50] Heym F, Etzold BJM, Kern C, Jess A. Analysis of evaporation and thermal decomposition of ionic liquids by thermogravimetrical analysis at ambient pressure and high vacuum. Green Chem 2011;13(6):1453.
[51] Villanueva M, Coronas A, García J, Salgado J. Thermal stability of ionic liquids for their application as new absorbents. Ind Eng Chem Res 2013;52(45):15718–27.
[52] Sovacool BK. Valuing the greenhouse gas emissions from nuclear power: a critical survey. Energy Policy 2008;36(8):2950–63.